

Basis Choice for Scalar-on-Function Regression with Applications to Near-Infrared Spectroscopy

Jonghun Baek, Jakob R. Juergens, Jonathan Willnow

11.02.2022

University of Bonn
Research Module in Econometrics and Statistics
Winter Semester 2021/2022

Contents

1	Introduction	3
2	Theory	3
2.1	Inner Products and Hilbert Spaces	4
2.2	Random Functions in the Hilbert Space of Square-Integrable Functions	4
2.3	Functional Data Sets	5
2.4	Representing a Function in terms of a Basis	5
2.5	Approximation and Smoothing via Basis Truncation	8
2.6	Karhunen-Loève Expansion and Empirical Eigenbases	9
2.7	Scalar-on-Function Regression	11
2.7.1	Estimation using Basis-Representation	12
2.7.2	Estimation using Functional Principal Components	13
3	Simulation Study	15
3.1	Motivation	15
3.2	Generating Similar Curves	16
3.3	Simulation setup	16
3.4	Results	18
3.4.1	Basis Expansion Regression	18
3.4.2	Functional Principal Component Regression	18
3.4.3	Interpretation and Relevance for Application	19
4	Application	20
4.1	Interpretation of Results	20
4.1.1	Basis Expansion Regression	20
4.1.2	Functional Principal Component Regression	21
5	Outlook	21
6	Appendix	23
6.1	Near-infrared (NIR) Spectroscopy	23
6.2	Basis Plots	24
6.3	Simulation Study Results	25
6.4	Additional Simulation	30
6.5	Simulation - Coefficient Function Estimates	31
6.6	Application Results	33
6.7	Application - Coefficient Function Estimates	35
7	Definitions and Proofs	35
7.1	Definition (Hilbert-Schmidt Integral Operator)	35
7.2	Lemma	36
7.3	Theorem (Karhunen-Loève Expansion)	37
8	Bibliography	40

1 Introduction

Functional Data Analysis (FDA), which has its roots in the work of Ulf Grenander and Kari Karhunen, is gaining more attention as researchers from different fields collect data that is functional in nature. Although classical statistical methods can often process this data, FDA has advantages in that it allows extracting information given by properties such as the smoothness of the underlying process or its derivatives (cf. Levitin et al. 2007). As Kokoszka and Reimherr 2017 describe, using methods from FDA should be considered when one variable of a given data set can be seen as smooth curves or functions. Therefore, data sets in FDA can include both realizations of scalar random variables and realizations of random functions. Examples of such curves are the absorption curves of electromagnetic radiation in the Near-infrared (NIR) spectrum by chemical samples.¹

This paper introduces Functional Linear Regression in a scalar-on-function setting. The distinct feature of this framework is that the regressor is a function, which makes a different approach to estimation necessary because the problem of estimating an unknown coefficient function is inherently infinite-dimensional. We then introduce two distinct ways of translating this infinite-dimensional problem into a finite-dimensional problem that can be addressed using theory from multivariate regression: First, a so-called basis expansion of the coefficient function, and second, functional principal component regression. Both of these methods are dependent on a parameter choice called a truncation parameter for a functional basis, and this paper focuses on exploring the selection of these parameters using cross-validation.

In Section 2, we introduce the necessary theoretical concepts, describe the estimation procedures, and address the theoretical importance of the truncation parameter. Section 3 contains a description of our Monte-Carlo Simulation, which aims to provide information on how to choose an appropriate functional basis and truncation parameter for the aforementioned methods. The application in Section 4 then uses the insights from theory and simulation to choose an appropriate basis for the estimation of octane numbers of gasoline samples based on Near-Infrared absorption curves. In Section 5, we give an outlook on possible extensions for this paper and describe the limitations of our approach.

2 Theory

To allow for scalar-on-function regression, it is necessary to extend some concepts from multivariate regression to the realm of infinite-dimensional objects, as the statistics derived from infinite-dimensional random functions cannot be defined on a finite-dimensional space. One integral concept that must be defined is random functions as a special case of random variables. Paraphrasing a definition by Bauer 2020, a random variable $X : \Omega \rightarrow \Omega'$ is an \mathcal{A} - \mathcal{A}' -measurable function, where (Ω, \mathcal{A}, P) is a probability space and (Ω', \mathcal{A}') is a measure space. The typical case for a random variable realizing in \mathbb{R} is $(\Omega', \mathcal{A}') = (\mathbb{R}, \mathcal{B})$, where \mathcal{B} is the canonical σ -algebra on the real numbers. As a first intuition for the concept of a random function, it is possible to imagine a similar concept where a random variable does not realize as an element of the real numbers but as a function in a function space. A formalization of this idea makes some more in-depth considerations necessary. The following theoretical introduction closely follows chapters 2.3 and 2.4 from Hsing and Eubank 2015 and chapters 4.4 and 4.6 from Kokoszka and Reimherr 2017.

¹For more details on Near-Infrared-Spectroscopy, refer to Appendix 6.1.

2.1 Inner Products and Hilbert Spaces

The first concept we will introduce is the concept of Hilbert spaces. To do so, we start from inner product spaces but restrict our analysis to vector spaces over \mathbb{R} for the sake of clarity. Let \mathbb{V} be a vector space over \mathbb{R} . Then, a function $\langle \cdot, \cdot \rangle : \mathbb{V} \times \mathbb{V} \rightarrow \mathbb{R}$ is called an inner product, if $\forall v, v_1, v_2 \in \mathbb{V}$ and $a_1, a_2 \in \mathbb{R}$ the following properties hold.

1. $\langle v, v \rangle \geq 0$
2. $\langle v, v \rangle = 0$ if $v = 0$
3. $\langle a_1 v_1 + a_2 v_2, v \rangle = a_1 \langle v_1, v \rangle + a_2 \langle v_2, v \rangle$
4. $\langle v_1, v_2 \rangle = \langle v_2, v_1 \rangle$

A vector space with an associated inner product is called an inner product space, and the inner product defines a norm and an associated distance on the vector space.

$$\|v\| = \langle v, v \rangle^{\frac{1}{2}} \quad \text{and} \quad d(v_1, v_2) = \langle v_2 - v_1, v_2 - v_1 \rangle^{\frac{1}{2}} \quad (1)$$

If the inner product space is complete with respect to the induced distance, it is called a Hilbert space, denoted \mathbb{H} in the following. To extend the known concept of a basis in a finite dimensional space to potentially infinite Hilbert spaces, it is necessary to define the closed span of a sequence of elements of \mathbb{H} . Recall that the span of a set of vectors $S \subseteq \mathbb{R}^P$ is given by

$$\text{span}(S) = \left\{ \sum_{i=1}^k \lambda_i v_i \mid k \in \mathbb{N}, v_i \in S, \lambda_i \in \mathbb{R} \right\} \quad (2)$$

The closed span $\overline{\text{span}}(S)$ of a sequence S in \mathbb{H} is defined as the closure of the span with respect to the distance induced by the norm and S is called a basis of \mathbb{H} if $\overline{\text{span}}(S) = \mathbb{H}$. It is called an orthonormal basis if, in addition, the following properties hold.

1. $\langle v_i, v_j \rangle = 0 \quad \forall v_i, v_j \in S \text{ for } i \neq j$
2. $\|v\| = 1 \quad \forall v \in S$

As in the case of a Banach space, each element of a Hilbert space can be expressed in terms of a corresponding basis. This can be done using a Fourier expansion of an element $x \in \mathbb{H}$ w.r.t. a basis $S = \{s_n\}$ as follows.

$$x = \sum_{j=1}^{\infty} \langle x, s_j \rangle s_j \quad (3)$$

Differing from the case of Banach spaces, these representations can be limits of series. As using an infinite number of basis functions is infeasible in applied contexts, an intuitive way to approximate elements in a Hilbert space is to use a truncated series.

$$x \approx \sum_{j=1}^K \langle x, s_j \rangle s_j \quad (4)$$

2.2 Random Functions in the Hilbert Space of Square-Integrable Functions

In functional data analysis, one Hilbert space of particular importance is the space of square-integrable functions on $[0, 1]$. Denoted by $\mathbb{L}^2[0, 1]$, this space consists of all μ -measurable functions $f(t)$ on $[0, 1]$

that fulfill the following condition in which μ denotes the Lebesgue-measure.

$$\|f\|_2 = \int_0^1 |f|^2 d\mu < \infty \quad (5)$$

This ensures that a random function has a finite second moment so that the variance and covariance functions can be defined. The inner product of $\mathbb{L}^2[0, 1]$ is defined by Equation 6.

$$\langle f_1, f_2 \rangle = \int_0^1 f_1 f_2 d\mu. \quad (6)$$

$\mathbb{L}^2[0, 1]$ is the function space that is most often used for theoretical considerations, but analogous constructions can be made for every closed interval of \mathbb{R} . A random function on $\mathbb{L}^2[0, 1]$ can then be defined formally as a function $X : \Omega \rightarrow \mathbb{L}^2[0, 1]$ defined on a probability space (Ω, \mathcal{A}, P) where Ω is a sample space with σ -algebra \mathcal{A} and a probability space P .

2.3 Functional Data Sets

If we take a random function $X(\omega)$ as defined in the previous section, then realizations $x(t)$ of $X(\omega)(t)$ are called sample curves of the random function. The presence of functional observations in a data set defines functional data sets. However, realizations of random functions are not typically observed in their functional form. Instead, each curve is observed at a discrete and typically large set of measurements points. Consider the case of a data set containing observations $x_i(t)$ of a random function $X(\omega)$

$$x_i(t_{i,j}) \in \mathbb{R}, \quad i = 1, \dots, N, \quad j = 1, \dots, J_i, \quad t_{i,j} \in [T_1, T_2] \quad (7)$$

Each curve $x_i(t)$ exists $\forall t \in [T_1, T_2]$, but is only observed at discrete measurement points $t_{i,j}$. These measurement points can be different for each sample curve. In this paper, we only consider the case where curves share their measuring points. To use the unique capabilities of functional data analysis with functional data obtained in this form, it is necessary to restore its functional structure. Therefore, methods such as basis representations will be introduced in the following parts of the Theory Section. As in the finite-dimensional setting, the concept of identically distributed and independent data is important for many aspects of functional data analysis. One example of i.i.d. curves could be Near-Infrared absorption spectra of gasoline samples where each sample is produced by the same production process and can therefore be interpreted as a realization of and i.i.d. random process itself. More information about this example can be found in Appendix 6.1.

2.4 Representing a Function in terms of a Basis

As previously described, a basis of a Hilbert space can be used to express its elements using the corresponding Fourier expansion. Let $\{\phi_i(t) \mid i \in \mathcal{I}\}$ be a basis used to express or approximate a realization $x(t)$ of $X(\omega)$. The following equation shows how a basis can be used to express a function as a weighted sum of its elements.

$$x(t) = \sum_{j \in \mathcal{I}} a_j \phi_j(t) \quad (8)$$

One very important question in this context is how the coefficients $a_j \quad j \in \mathcal{I}$ are derived given a function $x(t)$. For the purposes of this paper, this process will remain a black box, but detailed

information on the derivation of these coefficients can be found in chapter 4 of Ramsay and Silverman 2005. Three examples of bases often used to approximate elements of $\mathbb{L}^2[0, 1]$ in practice and in the later parts of this paper are explained in the following. Diagrams showing a number of basis functions from these bases are found in Section 6.2 of the Appendix.

Monomial Basis A straightforward idea to approximate functions in $\mathbb{L}^2[0, 1]$ is to take inspiration from the well-known Taylor expansion and to use monomials of increasing degree as a basis. For entire functions $f(t)$, such as polynomials, the exponential function, or trigonometric functions, we can express the function as a potentially infinite but converging sum of weighted monomials.

$$f(t) = \sum_{i=1}^{\infty} a_i t^i \quad \text{where} \quad a_i = \frac{f^{(i)}(0)}{i!} \quad (9)$$

The monomials are only a basis for the space of entire functions and not for $\mathbb{L}^2[0, 1]$. Nevertheless, even for functions that do not fall into this category, using a truncated Taylor expansion around a chosen point can lead to reasonable approximations around this specific point or even on \mathbb{R} as a whole. From this idea, it is natural to use the monomials as a potential basis for approximation.

As in the case of the Taylor expansion, it is not necessary to approximate a function around zero, as shown above. Instead, one can introduce a shift parameter. This shift parameter α is often chosen such that the monomials are evaluated at the center point of the domain of the function.

$$\phi_i^M(t) = (t - \alpha)^i, \quad i \in \mathcal{I} \quad (10)$$

Due to the implementation of our simulation, we will limit our paper to the case of $\alpha = 0$. However, a different choice of α could lead to improvements in the performance of the Monomial basis. As the monomials are not pairwise orthogonal, this basis is prone to collinearity problems, which can result in numerically unstable estimates. This restricts the number of basis functions that can be used in the estimation procedures limiting its ability to capture pronounced local peculiarities. These problems will be addressed in more detail in later parts of this paper. The limitation to a low number of monomials can additionally lead to undesirable behavior away from the point of evaluation (cf. Ramsay and Silverman 2005).

Fourier Basis In the same way the Monomial basis is connected to the Taylor series, the Fourier basis corresponds to the Fourier series, which can be used to decompose a periodic function into trigonometric functions. Equation 11 shows an example for a function with a period of 1.

$$s(x) = \frac{A_0}{2} + \sum_{i=1}^{\infty} A_i \cos(2\pi i x - \phi_i) = \frac{a_0}{2} + \sum_{i=1}^{\infty} [a_i \cos(2\pi i x) + b_i \sin(2\pi i x)] \quad (11)$$

Typically, the series is represented in the so-called amplitude-phase form. This, however, is impractical for the estimation procedures shown in the later parts of this paper due to the phase shift parameter. Therefore, rewriting the series in the sine-cosine form, as shown above, is necessary. The Fourier basis for $\mathbb{L}^2[0, 1]$ is thus given by the following sequence of functions defined on $[0, 1]$ directly corresponding to the terms of the sine-cosine form of the Fourier series.

$$\phi_i^F(x) = \begin{cases} 1 & \text{if } i = 1 \\ \sqrt{2} \cos(\pi i x) & \text{if } i \text{ is even} \\ \sqrt{2} \sin(\pi(i-1)x) & \text{otherwise} \end{cases} \quad (12)$$

To stay true to the original amplitude-phase form, it is reasonable to restrict the number of Fourier basis functions to odd-numbered values. The Fourier basis' elements exhibit a cyclical behavior which is useful to expand functions that represent a periodic or seasonal underlying process. The Fourier basis is especially suitable to expand functions with a similar curvature across the domain, generally resulting in uniformly smooth expansions. (cf. Ramsay and Silverman 2005)

B-spline Basis Following chapter 3.5 from Ramsay and Silverman 2005, splines are defined by first dividing an interval of interest $[\tau_0, \tau_L]$ into L subintervals of non-negative length divided by a non-decreasing sequence of points $(\tau_l)_{l=1, \dots, L-1}$ called knots. On each subinterval, a spline is a polynomial of order $m = n + 1$ where n is its degree. If there are no multiplicities in the set of knots, the polynomials on neighboring subintervals share derivatives up to order $m - 2$ at the boundary knot τ_l . A typical case that is often used in practice is an equidistant grid of knots. In some settings, however, it can be sensible to place multiple knots at the same value to replicate specific properties of the data structure, allowing for a reduced number of matching derivatives at the corresponding knots. For the purposes of this paper, we will focus on the case of equidistant knots without multiplicity at inner knots.

B-splines are a specific system of spline functions developed by Boor 1978 and are defined by a recursive procedure. Let $\phi_{l,m}^{BS}(x)$ $l \in \{1, \dots, L-1\}$ be a B-spline of order m for an interval $[\tau_0, \tau_L]$ and inner knots $\{\tau_l \mid l = 1, \dots, L-1\}$, then it is defined by the Cox-de Boor recursion formula as follows.

$$\phi_{l,0}^{BS}(x) = \begin{cases} 1 & \text{if } x \in [\tau_l, \tau_{l+1}) \\ 0 & \text{otherwise} \end{cases} \quad (13)$$

$$\phi_{l,m}^{BS}(x) = \frac{x - \tau_l}{\tau_{l+m} - \tau_l} \phi_{l,m-1}^{BS}(x) + \frac{\tau_{l+m+1} - x}{\tau_{l+m+1} - \tau_{l+1}} \phi_{l+1,m-1}^{BS}(x)$$

As this equation references knots that are not defined by the original vector of knots, implementations of this algorithm typically repeat the knots at the boundaries of the interval, τ_0 and τ_L , an additional m times. This padding of the knot vector then allows calculating every object that is needed for the definition of the basis over the original set of knots.

This, however, does not lead to a basis of $\mathbb{L}^2[0, 1]$ as the closed span of this finite sequence of functions is not equal to $\mathbb{L}^2[0, 1]$. To focus on specific approximation errors in the later parts of this paper, we will, however, assume that a B-spline basis representation of a function in $\mathbb{L}^2[0, 1]$ will serve as a sufficient approximation for an appropriately chosen number of B-spline basis functions. As the B-spline basis does not have infinitely many elements as the full Monomial or Fourier bases do, it is slightly misleading to speak of truncating the B-spline basis at a truncation parameter L in later parts of this paper. For the sake of keeping the notation reasonably concise, we will still keep this notation. However, by convention, truncating a B-spline basis at truncation parameter L shall mean using a B-spline basis consisting of L functions from this point on.

2.5 Approximation and Smoothing via Basis Truncation

Realized curves from a data set can be expressed in terms of a chosen functional basis. For this expansion, it is possible to use a complete basis of $\mathbb{L}^2[0, 1]$. In many cases, this is not a desirable approach as this expansion can introduce high amounts of variance or even lead to the approximation of noise in the sample curves, the latter being a typical case of overfitting. To combat this problem, smoothing methods such as, for example, acceleration penalties are employed to enforce a degree of smoothness in the analyzed curves. On the other hand, important information on the curves could be missed by smoothing the data too much by giving too much weight to a chosen penalty term leading to oversmoothing and loss of valuable information. This is a typical occurrence of the Bias-Variance tradeoff.

A different approach that is atypical in practice is to enforce smoothing by limiting the number of basis functions in the approximation of the functional objects. Here, the parameter of choice is not a weighting term for the penalty but the number of basis functions. Exploring this alternative smoothing method in two different estimation procedures is the main focus of this paper. A truncated basis expansion as described above is given in Equation 14.

$$X(\omega_0) = x(t) = \sum_{j \in \mathcal{I}} A_j(\omega_0) \phi_j(t) = \sum_{j=1}^L A_j(\omega_0) \phi_j(t) + \delta(t) \approx \sum_{j=1}^L A_j(\omega_0) \phi_j(t) \quad (14)$$

where $\delta(t)$ is the truncation error and $L \leq \max_{j \in \mathcal{I}}(j)$ for all $L \in \mathcal{I}$. In later parts, this approximation error is explicitly denoted in the derivation and then omitted for the final approximations. L can be chosen subjectively, but also through applying data-driven methods such as Cross-Validation. Figure 1 shows the effect of choosing different numbers of basis functions for one observation of the Near-Infrared Spectroscopy data set, which is used in the later parts of this paper and exemplifies the tradeoffs at the core of the truncation parameter choice.

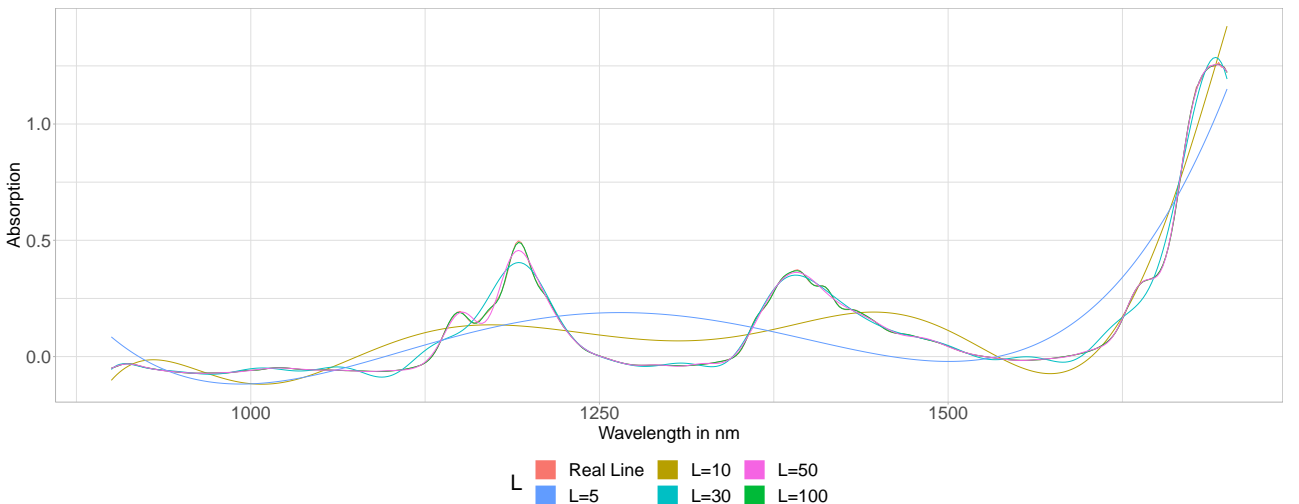


Figure 1: B-spline Approximations of NIR Absorption Spectra with different Basis Truncation Parameters

2.6 Karhunen-Loève Expansion and Empirical Eigenbases

Given a random function $X : \Omega \mapsto \mathbb{L}^2[0, 1]$, it is possible to represent its realizations in terms of the stochastic process. To do so, we define the mean and covariance functions of $X(\omega)$.

$$\mu(t) = \mathbb{E}[X(\omega)(t)] \quad (15)$$

$$c(t, s) = \mathbb{E}[(X(\omega)(t) - \mu(t))(X(\omega)(s) - \mu(s))] \quad (16)$$

where the $c : [0, 1] \times [0, 1] \rightarrow \mathbb{R}$ are Hilbert-Schmidt Kernels and K is a corresponding Hilbert-Schmidt integral operator² $K : \nu \rightarrow K\nu$ for $\nu \in \mathbb{L}^2[0, 1]$ defined by

$$[K\nu](t) = \int_0^1 c(t, s)\nu(s)ds = \lambda\nu(t) \quad (17)$$

Then, the operator K has orthonormal basis functions $\nu^m \in \mathbb{L}^2[0, 1]$, each corresponding to an Eigenvalue λ^m since it is a positive compact self-adjoint operator (cf. Alexanderian 2015). Theoretical considerations lead to the result that X can be represented in the following form, called its Karhunen-Loève expansion.³

$$X(\omega)(t) = \mu(t) + \sum_{m=1}^{\infty} \xi^m(\omega)\nu^m(t), \quad \xi^m(\omega) = \int_0^1 (X(\omega)(s) - \mu(s))\nu^m(s)ds \quad (18)$$

where the ν^m are defined by the countable set of solutions $\{(\lambda^m, \nu^m) \mid m \in \mathbb{N}\}$ of Equation 17 and the random variables $\xi^m(\omega)$ satisfy the following properties.

1. $\mathbb{E}[\xi^m(\omega)] = 0$
2. $Cov(\xi^m(\omega), \xi^n(\omega)) = 0$ if $m \neq n$
3. $Var(\xi^m(\omega)) = \lambda^m$

As in the well-known setting of principal component analysis, the Eigenvalues correspond to the variance in the random function explained by the corresponding Eigenfunction. Therefore, ordering the Eigenfunctions according to their corresponding Eigenvalues $\lambda^1 \geq \lambda^2 \geq \dots \geq 0$ is useful for approximation purposes. Due to this property, a functional observation can often be approximated well by using a limited number of the Eigenfunctions of its generating random process. Moreover, our data generating process for the simulation study is based on this property as explained in Section 3.2. In the scalar setting, a similar consideration leads to the concept of principal components, which can be extended to the functional setting. Let $\{x_1(t), \dots, x_n(t)\}$ be a set of i.i.d. realizations generated by a random function $X(\omega) \mapsto \mathbb{L}^2[0, 1]$. Define the following sample analogs for the mean and covariance functions.

$$\hat{\mu}(t) = \frac{1}{N} \sum_{i=1}^N x_i(t) \quad (19)$$

$$\hat{c}(t, s) = \frac{1}{N} \sum_{i=1}^N (x_i(t) - \hat{\mu}(t))(x_i(s) - \hat{\mu}(s)) \quad (20)$$

²Definitions of Hilbert-Schmidt Kernel and Integral Operator are provided in Appendix 7.1.

³Proofs for these theorems are provided in Appendix 7.2 and 7.3.

With these it is possible to derive a set of sample analogs $\{(\hat{\lambda}^m, \hat{\nu}^m) \mid m = 1, \dots, N-1\}$ for $\{(\lambda^m, \nu^m) \mid m = 1, 2, \dots\}$ as the solutions of the following equation.

$$\int_0^1 \hat{c}(t, s) \hat{\nu}(s) ds = \hat{\lambda} \hat{\nu}(t) \quad (21)$$

In the following, we will call the $\hat{\nu}^m(s)$ functional principal components to distinguish the sample analogs from the theoretical Eigenfunctions $\nu^m(s)$. As in the case of ordinary principal components, the number of functional principal components corresponding to non-zero Eigenvalues is limited (cf. chapter 8.2.3 Ramsay and Silverman 2005). As each curve is infinite-dimensional, there is no upper limit to this number due to the dimensionality. However, the number of curves still imposes an upper limit of $N-1$ non-zero Eigenvalues, where N is the number of curves in the data set. These sample analogs naturally lead to the following representation of each sample curve $x_i(t)$.

$$x_i(t) = \hat{\mu}(t) + \sum_{j=1}^{N-1} \hat{\xi}_i^m \hat{\nu}^m(t) \quad (22)$$

where the $\hat{\xi}_i^m$ are derived as

$$\hat{\xi}_i^m(\omega) = \langle x_i - \hat{\mu}, \hat{\nu}^m \rangle = \int_0^1 (x_i(s) - \hat{\mu}(s)) \hat{\nu}^m(s) ds \quad (23)$$

In reality, these calculations are often implemented using basis representations of both the functional principal components $\hat{\nu}^m$ and the observations $x_i(t)$ leading to the following representation. For the sake of clarity, the following equation assumes that the bases used for the expansion of both the observations and the coefficient function are proper bases of $\mathbb{L}^2[0, 1]$ and can therefore be used to express the corresponding objects exactly.

$$\begin{aligned} \hat{\xi}_i^m &= \int_0^1 (x_i(s) - \hat{\mu}(s)) \hat{\nu}^m(s) ds = \int_0^1 \left(\sum_{j \in \mathcal{I}} a_{i,j} \phi_j(s) \right) \left(\sum_{k \in \mathcal{L}} d_k^m \psi_k(s) \right) ds \\ &= \int_0^1 \left(\sum_{j=1}^J a_{i,j} \phi_j(s) + \delta_i^J(s) \right) \left(\sum_{k=1}^K d_k^m \psi_k(s) + \delta_\nu^{m,K}(s) \right) ds \\ &= \sum_{j=1}^J \left[a_{i,j} \sum_{k=1}^K d_k^m \int_0^1 \phi_j(s) \psi_k(s) ds \right] + \sum_{k=1}^K d_k^m \int_0^1 \delta_i^J(s) \psi_k(s) ds \\ &\quad + \sum_{j=1}^J a_{i,j} \int_0^1 \phi_j(s) \delta_\nu^{m,K}(s) ds + \int_0^1 \delta_i^J(s) \delta_\nu^{m,K}(s) ds \end{aligned} \quad (24)$$

In practice, a typical choice is to use the same basis $(\phi_j(t))_{j \in \mathcal{I}}$ and the same truncation parameter L for the basis expansion of the demeaned observations $(x_i(t) - \hat{\mu}(t))$ and the functional principal components $\hat{\nu}^m$. This leads to the following simplification of Equation 24.

$$\begin{aligned} \hat{\xi}_i^m &= \sum_{j=1}^L \left[a_{i,j} \sum_{k=1}^L d_k^m \int_0^1 \phi_j(s) \phi_k(s) ds \right] + \sum_{k=1}^L d_k^m \int_0^1 \delta_i^L(s) \phi_k(s) ds \\ &\quad + \sum_{j=1}^L a_{i,j} \int_0^1 \phi_j(s) \delta_\nu^{m,L}(s) ds + \int_0^1 \delta_i^L(s) \delta_\nu^{m,L}(s) ds \end{aligned} \quad (25)$$

And we can define the following objects:

$$\tilde{\xi}_i^{m,L} := \sum_{j=1}^L \left[a_{i,j} \sum_{k=1}^L d_k^m \int_0^1 \phi_j(s) \phi_k(s) ds \right] \quad \delta_{\xi,i}^L := \hat{\xi}_i^m - \tilde{\xi}_i^{m,L} \quad (26)$$

$$\tilde{\nu}^{m,L}(t) := \sum_{k=1}^L d_k^m \phi_k(t) \quad \delta_{\nu}^{m,L}(t) := \hat{\nu}^m(t) - \tilde{\nu}^{m,L}(t) \quad (27)$$

This method of deriving or approximating the Eigenfunctions and scores from a data set is introduced in Ramsay and Silverman 2005 (chapter 8.4.2) and implemented in the R-package `fda`. The following considerations and results of the simulation study might serve as information about the performance of this method in a scenario where a limited number of basis functions is provided to the method instead of using more conventional smoothing approaches.

2.7 Scalar-on-Function Regression

In the simple scalar setting, one of the essential tools in econometrics is linear regression. Its goal is twofold: to gain information about the dependency between variables and allow for prediction. To motivate the jump from multivariate regression to scalar-on-function regression, assume a data generating process as follows.

$$Y = X\beta + \epsilon \quad (28)$$

Here, Y is the vector of response variables, X is the matrix containing the corresponding regressors in its columns, and $\beta = (\beta_0, \beta_1, \dots, \beta_p)'$ is the vector containing the unknown coefficients. In this finite-dimensional setting, one important question is how to estimate the unknown coefficients β . The most famous estimator in all of econometrics, the Ordinary Least Squares (OLS) estimator, fulfills this purpose under a set of assumptions.

$$\hat{\beta}_{OLS} = (X'X)^{-1}X'Y \quad (29)$$

The concept of linear regression can be extended to the setting of functional data, where a scalar response variable is assumed to be dependent on a functional regressor. Even though integrating over the product of an observation with the coefficient function is not the only functional that can be used to create a data generating process involving functional observations, it is the most typical as it naturally extends the intuition from multiple linear regression to the realm of infinite-dimensional objects. Therefore, we will always assume a data generating process as follows in this paper.

$$Y(\omega) = \alpha + \int_0^1 \beta(s)X(\omega)(s)ds + \epsilon(\omega) \quad (30)$$

Similar to the finite-dimensional setting, an interesting question is how to estimate the unknown coefficient function $\beta(t)$ given a data set containing realizations of a random function and associated scalar response variables. However, a simple extension of the OLS estimator to allow for infinite-dimensional objects is not possible. Therefore, other options have to be considered, two of which will be explained in the following.

2.7.1 Estimation using Basis-Representation

The most common way to make this problem tractable is via a basis representation of $\beta(t)$. Therefore, let $\{\phi_i(t) \mid i \in \mathcal{I}\}$ be a basis of $\mathbb{L}^2[0, 1]$ and represent $\beta(t)$ in terms of this basis.

$$\beta(t) = \sum_{j \in \mathcal{I}} b_j \phi_j(t) \quad (31)$$

This enables us to write equation 30 using this representation to obtain a formulation as a sum of scalar random variables $Z_j(\omega)$.

$$\begin{aligned} Y(\omega) &= \alpha + \int_0^1 \beta(s) X(\omega)(s) ds + \epsilon(\omega) = \alpha + \int_0^1 \left[\left(\sum_{j \in \mathcal{I}} b_j \phi_j(s) \right) X(\omega)(s) \right] ds + \epsilon(\omega) \\ &= \alpha + \sum_{j \in \mathcal{I}} \left[b_j \int_0^1 X(\omega)(s) \phi_j(s) ds \right] + \epsilon(\omega) = \alpha + \sum_{j \in \mathcal{I}} b_j Z_j(\omega) + \epsilon(\omega) \end{aligned} \quad (32)$$

This representation translates the original problem of regressing a scalar on a continuously observed function to a problem where a scalar is regressed on what is possibly a countably infinite sequence of regressors. Using a truncation of the basis at some parameter J can be used to make this problem tractable if we assume that the approximation error created by this truncation is small.

$$\begin{aligned} Y(\omega) &= \alpha + \int_0^1 \left[\left(\sum_{j=1}^J b_j \phi_j(s) + \delta_\beta^J(s) \right) X(\omega)(s) \right] ds + \epsilon(\omega) \\ &= \alpha + \sum_{j=1}^J b_j \int_0^1 \phi_j(s) X(\omega)(s) ds + \int_0^1 \delta_\beta^J(s) X(\omega)(s) ds + \epsilon(\omega) \end{aligned} \quad (33)$$

In practice, it is common to not only express the coefficient function in terms of a basis but also the observations. Therefore two bases $((\phi_j(t))_{j \in \mathcal{I}})$ and $(\psi_k(t))_{k \in \mathcal{L}})$ and two corresponding truncation parameters (J and K) can be chosen. This leads to the following representation.

$$\begin{aligned} Y(\omega) &= \alpha + \int_0^1 \beta(s) X(\omega)(s) ds + \epsilon(\omega) = \alpha + \int_0^1 \left[\left(\sum_{j \in \mathcal{I}} b_j \phi_j(s) \right) \left(\sum_{k \in \mathcal{L}} a_k(\omega) \psi_k(s) \right) \right] ds + \epsilon(\omega) \\ &= \alpha + \int_0^1 \left[\left(\sum_{j=1}^J b_j \phi_j(s) + \delta_\beta^J(s) \right) \left(\sum_{k=1}^K a_k(\omega) \psi_k(s) + \delta_X^K(\omega)(s) \right) \right] ds + \epsilon(\omega) \\ &= \alpha + \sum_{j=1}^J b_j \left[\sum_{k=1}^K a_k(\omega) \int_0^1 \phi_j(s) \psi_k(s) ds \right] + \sum_{j=1}^J b_j \int_0^1 \phi_j(s) \delta_X^K(\omega)(s) ds \\ &\quad + \sum_{k=1}^K a_k(\omega) \int_0^1 \delta_\beta^J(s) \phi_j(s) ds + \epsilon(\omega) + \int_0^1 \delta_\beta^J(s) \delta_X^K(\omega)(s) ds \end{aligned} \quad (34)$$

A typical choice in this scenario is to use the same functional basis $(\phi_j(t))_{j \in \mathcal{I}}$ and the same truncation parameter L for both the coefficient function and the approximation of the observations. Using the following notation

$$\tilde{Z}_j(\omega) = \sum_{k=1}^L \left[a_k(\omega) \int_0^1 \phi_j(s) \phi_k(s) ds \right] \quad j = 1, \dots, L \quad (35)$$

this leads to a considerable simplification of Equation 2.7.1.

$$\begin{aligned}
Y(\omega) &= \alpha + \sum_{j=1}^L b_j \tilde{Z}_j(\omega) + \sum_{j=1}^L b_j \int_0^1 \phi_j(s) \delta_X^L(\omega)(s) ds \\
&\quad + \sum_{k=1}^L a_k \int_0^1 \delta_\beta^L(s) \phi_j(s) ds + \epsilon(\omega) + \int_0^1 \delta_\beta^L(s) \delta_X^L(\omega)(s) ds + \epsilon(\omega) \\
&\approx \alpha + \sum_{j=1}^J b_j \tilde{Z}_j(\omega) + \epsilon(\omega)
\end{aligned} \tag{36}$$

A model in the form of Equation 36 naturally lends itself to be estimated using theory from multivariate linear regression. Define therefore the following objects

$$Y = \begin{pmatrix} y_1 \\ \vdots \\ y_n \end{pmatrix}, \quad Z = \begin{pmatrix} 1 & \tilde{Z}_{1,1} & \dots & \tilde{Z}_{1,J} \\ \vdots & \vdots & \ddots & \vdots \\ 1 & \tilde{Z}_{N,1} & \dots & \tilde{Z}_{N,J} \end{pmatrix} \tag{37}$$

Then an OLS estimator can be calculated in the usual way to obtain an estimate for the values of α and b_j , and an estimate of the coefficient function can be derived accordingly.

$$b^L = (Z'Z)^{-1} Z'Y \in \mathbb{R}^{L+1} \quad \hat{\alpha} = b_1^L \quad \hat{\beta}^L(t) = \sum_{j=1}^J b_{j+1}^L \phi_j(t) \tag{38}$$

The performance of this estimation procedure depends in part on the quality of the approximation in Equation 36. Therefore, it is interesting to think about when the approximation error is small. Due to the nature of a basis representation, the approximation error can only decrease with an increasing number of basis functions. However, contrary to this effect are the potential benefits of introducing some amount of smoothing into the procedure, making it not intuitively clear, what the effects of different choices for the number of basis functions might be.

2.7.2 Estimation using Functional Principal Components

Using the Karhunen-Loève Expansion to represent $X(\omega)$, it is also possible to express the data generating process in terms of the Eigenfunctions of $X(\omega)(t)$.

$$\begin{aligned}
Y(\omega) &= \alpha + \int_0^1 \textcolor{red}{X}(\omega)(s) \beta(s) ds + \epsilon(\omega) = \alpha + \int_0^1 \left(\mu(s) + \sum_{m=1}^{\infty} \xi^m(\omega) \nu^m(s) \right) \beta(s) ds + \epsilon(\omega) \\
&= \alpha + \int_0^1 \mu(s) \beta(s) ds + \sum_{m=1}^{\infty} \xi^m(\omega) \int_0^1 \nu^m(s) \beta(s) ds + \epsilon(\omega) = \bar{\alpha} + \sum_{m=1}^{\infty} \xi^m(\omega) \beta^m + \epsilon(\omega)
\end{aligned} \tag{39}$$

As these theoretical Eigenfunctions and Eigenvalues are typically unknown, the corresponding equation in sample analogs is more interesting as a representation of an observation.

$$\begin{aligned}
y_i &= \alpha + \int_0^1 \textcolor{red}{x}_i(s) \beta(s) ds + \epsilon_i = \alpha + \int_0^1 \left(\hat{\mu}(s) + \sum_{m=1}^{N-1} \hat{\xi}_i^m \hat{\nu}^m(s) \right) \beta(s) ds + \epsilon_i \\
&= \alpha + \int_0^1 \hat{\mu}(s) \beta(s) ds + \sum_{m=1}^{N-1} \hat{\xi}_i^m \int_0^1 \hat{\nu}^m(s) \beta(s) ds + \epsilon_i = \bar{\alpha} + \sum_{m=1}^{N-1} \hat{\xi}_i^m \hat{\beta}^m + \epsilon_i
\end{aligned} \tag{40}$$

This, however, is a simplification as in most implementations, the coefficient function and the principal components are also expressed or derived in terms of a basis. Introducing both concepts one step at a time leads to the following complication if we first introduce an expansion of the coefficient function.

$$\begin{aligned}
y_i &= \alpha + \int_0^1 \mathbf{x}_i(s) \beta(s) ds + \epsilon_i = \alpha + \int_0^1 \left(\hat{\mu}(s) + \sum_{m=1}^{N-1} \hat{\xi}_i^m \hat{\nu}^m(s) \right) \left(\sum_{j \in \mathcal{I}} b_j \phi_j(s) \right) ds + \epsilon_i \\
&= \alpha + \int_0^1 \left[\sum_{j \in \mathcal{I}} b_j \phi_j(s) \hat{\mu}(s) + \sum_{m=1}^{N-1} \left[\hat{\xi}_i^m \sum_{j \in \mathcal{I}} b_j \hat{\nu}^m(s) \phi_j(s) \right] \right] ds + \epsilon_i \\
&= \alpha + \sum_{j \in \mathcal{I}} b_j \int_0^1 \phi_j(s) \hat{\mu}(s) ds + \sum_{m=1}^{N-1} \left[\hat{\xi}_i^m \sum_{j \in \mathcal{I}} b_j \int_0^1 \hat{\nu}^m(s) \phi_j(s) ds \right] + \epsilon_i
\end{aligned} \tag{41}$$

Truncating the basis used for expansion of the coefficient function already introduces an approximation error.

$$\begin{aligned}
y_i &= \alpha + \int_0^1 \left(\hat{\mu}(s) + \sum_{m=1}^{N-1} \hat{\xi}_i^m \hat{\nu}^m(s) \right) \left(\sum_{j=1}^J b_j \phi_j(s) + \delta_\beta^J(s) \right) ds + \epsilon_i \\
&= \alpha + \sum_{j=1}^J b_j \int_0^1 \phi_j(s) \hat{\mu}(s) ds + \int_0^1 \delta_\beta^J(s) \hat{\mu}(s) ds + \sum_{m=1}^{N-1} \left[\hat{\xi}_i^m \sum_{j=1}^J b_j \int_0^1 \hat{\nu}^m(s) \phi_j(s) ds \right] \\
&\quad + \sum_{m=1}^{N-1} \left[\hat{\xi}_i^m \int_0^1 \hat{\nu}^m(s) \delta_\beta^J(s) ds \right] + \epsilon_i
\end{aligned} \tag{42}$$

If we additionally derive and approximate the principal components and corresponding scores using a truncated basis representation as in Equation 25, we obtain the following. To not complicate things more than necessary, the following equation assumes that the same basis $(\phi_j(t))_{j \in \mathcal{I}}$ was used in the derivation of the principal components and the expansion of the coefficient function. Additionally, the following approximation truncates the basis for the expansion of the coefficient function at the same parameter L that was used for the approximation of the principal components and scores.

For convenience, define the following notation:

$$\tilde{\alpha}^L = \alpha + \sum_{j=1}^L b_j \int_0^1 \phi_j(s) \hat{\mu}(s) ds + \int_0^1 \delta_\beta^L(s) \hat{\mu}(s) ds \tag{43}$$

Then Equation 42 can be expressed as follows.

$$\begin{aligned}
y_i &= \tilde{\alpha}^L + \sum_{m=1}^{N-1} \left[\left(\tilde{\xi}_i^{m,L} + \delta_{\xi,i}^{m,L} \right) \sum_{j=1}^L b_j \int_0^1 (\tilde{\nu}^{m,L}(s) + \delta_\nu^{m,L}(s)) \phi_j(s) ds \right] + \epsilon_i \\
&= \tilde{\alpha}^L + \sum_{m=1}^{N-1} \left[\tilde{\xi}_i^{m,L} \sum_{j=1}^L b_j \int_0^1 \tilde{\nu}^{m,L}(s) \phi_j(s) ds \right] + \sum_{m=1}^{N-1} \left[\tilde{\xi}_i^{m,L} \sum_{j=1}^L b_j \int_0^1 \delta_\nu^{m,L}(s) \phi_j(s) ds \right] \\
&\quad + \sum_{m=1}^{N-1} \left[\delta_{\xi,i}^{m,L} \sum_{j=1}^L b_j \int_0^1 \tilde{\nu}^{m,L}(s) \phi_j(s) ds \right] + \sum_{m=1}^{N-1} \left[\delta_{\xi,i}^{m,L} \sum_{j=1}^L b_j \int_0^1 \delta_\nu^{m,L}(s) \phi_j(s) ds \right] + \epsilon_i \\
&\approx \tilde{\alpha}^L + \sum_{m=1}^{N-1} \left[\tilde{\xi}_i^{m,L} \sum_{j=1}^L b_j \int_0^1 \tilde{\nu}^{m,L}(s) \phi_j(s) ds \right] + \epsilon_i
\end{aligned} \tag{44}$$

The parameter $M \in \{1, \dots, N-1\}$ corresponds to the chosen number of principal components and therefore constitutes another choice in the approximation. Using only M functional principal components leads to the following approximation.

$$y_i \approx \tilde{\alpha}^L + \sum_{m=1}^M \left[\tilde{\xi}_i^{m,L} \sum_{j=1}^L b_j \int_0^1 \tilde{\nu}^{m,L}(s) \phi_j(s) ds \right] + \epsilon_i = \tilde{\alpha}^L + \sum_{m=1}^M \tilde{\xi}_i^{m,L} \bar{b}^{m,L} + \epsilon_i \quad (45)$$

As in the previous section, this equation lends itself for estimation with OLS and we can define the following objects.

$$Y = \begin{pmatrix} y_1 \\ \vdots \\ y_n \end{pmatrix}, \quad Z = \begin{pmatrix} 1 & \tilde{\xi}_1^{1,L} & \dots & \tilde{\xi}_1^{M,L} \\ \vdots & \vdots & \ddots & \vdots \\ 1 & \tilde{\xi}_N^{1,L} & \dots & \tilde{\xi}_N^{M,L} \end{pmatrix} \quad (46)$$

We can then derive the following estimator for $\tilde{\alpha}^L$ and $\bar{b}^{m,L}$ $m = 1, \dots, M$

$$\tilde{b}^{L,M} = (Z'Z)^{-1} Z'Y \in \mathbb{R}^{M+1} \quad \hat{\alpha} = \tilde{b}_1^{L,M} \quad \hat{\beta}(t) = \sum_{m=1}^M \tilde{b}_{m+1}^{L,M} \tilde{\nu}^{m,L}(t) \quad (47)$$

As in the previous case, the performance of this estimation depends in parts on the quality of the approximation made during the derivation of this estimator. Here, the interactions are even more complicated. Even though the approximations exhibit smaller errors when a larger number of basis functions is used, the interplay of smoothing in the construction of the functional principal components and the choice of a number of FPC's to be used in the linear regression makes the behavior of this estimator difficult to predict.

3 Simulation Study

3.1 Motivation

In the simulation study, we deviate from the standard simulation setting. Instead of generating data from scratch, we use the gasoline data, which consists of 60 samples of Near-infrared (NIR) absorption spectra measured in increments of 2 nm from 900 to 1,700 nm, and a response variable, the octane rating. We chose this setup to improve the approach towards the application in which we predict the octane ratings from the gasoline data set.

To exploit the regularity of the curves of the spectra, we introduced different basis functions in Section 2.4 and demonstrated the importance of the truncation parameter K for the estimation in Section 2.7. For the simulation study, we rely on the introduced estimation strategies with the introduced basis functions and focus on choosing the truncation parameter L as well as the number of FPC's, which is possibly affected by L , by ten-fold cross-validation using the prediction mean-squared error. The number of FPC's is in practice chosen by using the lowest number of FPC's that explains a specified proportion of variance (cf. Kokoszka and Reimherr 2017), which might not be optimal since FPC's with smaller Eigenvalues may have a more significant influence on the prediction (cf. Jolliffe 1982). This might apply to this simulation too since certain Eigenfunctions could correspond to certain chemical combinations and overtones in the absorption bands of the spectrum that could have high predictive power, but explain only little variability in the NIR curves shown in Appendix 6.1.

This setup differs from the often used penalized functional regression as described by Goldsmith et al. 2011 in which an explicit smoothness constraint is used to tune the smoothness of the estimator $\hat{\beta}(t)$ while setting the L sufficiently high. This would avoid the heavy computations of validating the best value for L , which we will conduct in the simulation. To provide intuition in this approach, let

$$PSSE_{\lambda}(\alpha, \beta) = \sum_{i=1}^N \left[Y_i - \alpha - \int_0^1 \beta(t) X_i(t) dt \right]^2 + \lambda \int [D^m \beta(t)]^2 dt \quad (48)$$

denote the penalized residual sum of squares as notated by Ramsay and Silverman 2005 for the derivative of order m . A typical choice is the second derivative, as highly variable functions are expected to exhibit large second derivatives and therefore a larger penalty. The smoothing parameter λ is set to minimize the $PSSE_{\lambda}(\alpha, \beta)$, which can be archived by different criteria as shown in Thomas C.M. Lee 2003.

3.2 Generating Similar Curves

To avoid small sample problems, we generated 200 similar curves, NIR_{sim} , from the spectra of the gasoline data set, NIR , motivated by Karhunen-Loève Expansion. First, the initial curves are expressed in terms of a cubic B-spline basis which is created using 50 knots. In the R implementation of the fda package, these 50 knots account for 52 basis functions ($50 + 4 - 2$). These smooth curves are then centered before applying the Karhunen-Loève Expansion. We assume that the scores follow a normal distribution, so the new realizations for the scores are drawn from a multivariate normal distribution $\xi = (\xi^1, \dots, \xi^M)' \sim \mathcal{N}(0_M, \text{diag}(\hat{\lambda}^1, \dots, \hat{\lambda}^M))$. Finally, we obtain the generated curves NIR_{sim} as

$$\hat{X}(\omega)(t) = \hat{\mu}(t) + \sum_{m=1}^M \xi^m(\omega) \tilde{\nu}^{m,L}(t) \quad (49)$$

where $\hat{X}(\omega)(t)$, $\hat{\mu}(t)$ and $\tilde{\nu}^{m,L}(t)$ are approximated as vectors in \mathbb{R}^{401} for $M = 30$ FPC's.

3.3 Simulation setup

The simulation study follows Reiss and Ogden 2007 as a guideline. Two different true coefficient functions, $f_1(t)$ and $f_2(t)$, that differ in their smoothness are created to compare the introduced methods with differing true coefficient functions:

$$f_1(t) = 401 [2 \sin(0.5\pi t) + 4 \sin(1.5\pi t) + 5 \sin(2.5\pi t)] \quad (50)$$

$$f_2(t) = 401 \left[1.5 \exp\left(\frac{-0.5(t-0.3)^2}{0.02^2}\right) - 4 \exp\left(\frac{-0.5(t-0.45)^2}{0.015^2}\right) + 8 \exp\left(\frac{-0.5(t-0.6)^2}{0.02^2}\right) - \exp\left(\frac{-0.5(t-0.8)^2}{0.03^2}\right) \right] \quad (51)$$

The function $f_2(t)$ was generated by referring to Cardot 2002 while function $f_1(t)$ directly follows Reiss and Ogden 2007.



Figure 2: $f_1(t)$, smooth function



Figure 3: $f_2(t)$, bumpy function

Two different error-terms ϵ were created by first generating an i.i.d. standard normal error term and then multiplying it by two error variations σ_e . The error variations represent different signal-to-noise ratios of the responses to test the methods with low and high amounts of noise in the responses. They are created such that the squared multiple correlation coefficient $R^2 = \text{var}(\langle X, f \rangle) / (\text{var}(\langle X, f \rangle) + \sigma_e^2)$ is equal to 0.9 and 0.6. The two error terms are then used to generate two sets of responses for $f \in \{f_1(t), f_2(t)\}$

$$\begin{aligned} Y_{1,f} &= \langle NIR_{sim}, f \rangle + Z \left[\frac{\text{var}(\langle NIR_{sim}, f \rangle)}{0.9} - \text{var}(\langle NIR_{sim}, f \rangle) \right] \\ Y_{2,f} &= \langle NIR_{sim}, f \rangle + Z \left[\frac{\text{var}(\langle NIR_{sim}, f \rangle)}{0.6} - \text{var}(\langle NIR_{sim}, f \rangle) \right] \end{aligned} \quad (52)$$

where $Z \sim \mathcal{N}(0, 1)$. In total, we created four combinations, using the two true coefficient functions and the two error terms. These four combinations are then used with a different number of Monomial basis functions $\in \{1, 2, \dots, 6\}$, cubic B-spline basis-function $\{5, 6, \dots, 18\}$ and Fourier functions $\{1, 3, \dots, 25\}$ to predict the generated responses using the basis expansion approach and the FPCR approach.

To obtain valid out of sample properties for the FPCR, within each of the ten ten-fold cross-validation splits, we first calculated the first n_{FPC} FPC's for $n_{FPC} \in \{2, 3, 4\}$ of the training set \mathcal{T} , which was smoothed with the respective basis function specification. The approximated Eigenfunctions $\tilde{\nu}^{m,L,\mathcal{T}}$ are then used to estimate the scores of the holdout set \mathcal{H} , $\tilde{\xi}_i^{m,L,\mathcal{H}}$ by Equation 53.

$$\tilde{\xi}_i^{m,\mathcal{H},L} = \int_0^1 \left(\sum_{j=1}^L a_{i,j}^{\mathcal{H}} \phi_j(s) \right) \left(\sum_{k=1}^L d_k^{m,L,\mathcal{T}} \phi_k(s) \right) ds = \sum_{j=1}^L \left[a_{i,j}^{\mathcal{H}} \sum_{k=1}^L d_k^{m,\mathcal{T}} \int_0^1 \phi_j(s) \phi_k(s) ds \right] \quad (53)$$

where

$$\begin{aligned} (X_i^{\mathcal{H}}(t) - \hat{\mu}^{\mathcal{T}}(t)) &= \sum_{j \in \mathcal{L}} a_{i,j}^{\mathcal{H}} \phi_j(t) = \sum_{j=1}^L a_{i,j}^{\mathcal{H}} \phi_j(t) + \delta_i^{L,\mathcal{H}}(t) \approx \sum_{j=1}^L a_{i,j}^{\mathcal{H}} \phi_j(t) \\ \tilde{\nu}^{m,L,\mathcal{T}} &= \sum_{k=1}^L d_k^{m,L,\mathcal{T}} \phi_k(s) \end{aligned} \quad (54)$$

In total, 5000 repetitions were conducted for each specified model, basis system and basis function. The models are denoted as a combination of the function $f \in \{f_1(t), f_2(t)\}$ and created responses $Y \in \{Y_1, Y_2\}$.

3.4 Results

The discussed results and figures of $\hat{\beta}(t)$ for the simulation can be found in Appendix 6.3 and 6.5.

3.4.1 Basis Expansion Regression

The following results originate from the Estimation using Basis-Representation, in which we transform the smooth curves to perform scalar-on-function regression. Examining the results, it appears that the cross-validated mean squared prediction error (MSPE) exhibits a convex behavior in the number of basis functions.

Monomial Basis Due to the increasing collinearity problems for higher numbers of Monomial basis functions, simulations were conducted up until the sixth monomial, which already shows signs of numerical instability. For reasons outlined in 2.4 **This is not explained anymore in 2.4**, they seem suited for f_1 , where it shows a better performance than B-splines for this coefficient function. A hypothesis for this could be that f_1 is an entire function, which can be well approximated with a power series. In the case of f_2 , this basis shows the weakest performance out of all basis, for which the plots in Figures 11 and 12 provide evidence. It seems like $\hat{\beta}(t)$ is not changing in the amount of noise and shows exaggerated behavior at the boundaries. This weakness is especially pronounced in the MSPE for f_2, Y_1 . For f_1 , the simulation selects 5(3) and for f_2 5(5) Monomial basis functions for the high(low) signal-to-noise ratio.

B-spline Basis Simulations with B-spline basis functions were possible from 4 to 18 since from 18 onward, the simulations were running into problems of numerical instability **since the functions are inherently not orthogonal to each other**. Function f_1 requires 5(4) B-spline basis functions for the high(low) signal-to-noise ratio to obtain the best fit for the B-spline basis and shows the worst performance of the three bases. An explanation might be its overripe behavior at the boundaries and the exaggeration of the peculiarities of f_1 (Figures 9 and 10), which is especially pronounced for the lower signal-to-noise ratio. For f_2 , 11(6) B-spline basis functions are chosen for the high(low) signal-to-noise ratio. The B-spline basis outperforms the Monomial basis in f_2 but comes second to the Fourier basis. While the basis seems to recognize the peculiarities in f_2, Y_1 , it seems to struggle for the noisy responses in f_2, Y_2 (Figures 11 and 12). With the low signal-to-noise ratio in the responses, the simulation chooses a smaller number of basis functions, which could prevent fitting this scalar noise using $\hat{\beta}(t)$.

Fourier Basis For f_1 , the simulation chooses a smaller number of Fourier basis functions, 5(3) and a higher number for f_2 , 9(7) for the setup with the high(low) signal-to-noise ratio. As for the B-splines basis functions, the simulation chooses a smaller number of basis functions for the noisy responses and a higher number for the high signal-to-noise responses. The Fourier basis functions perform the best for each setup for the basis expansion regression. Several reasons could contribute to this: First, especially f_1 shows similar curvature order across the domain while the curvature of f_2 does at least not display any erratic jumps. Second, both functions feature periodic behavior. Third, f_2 does have the same value at the start- and the end of the interval, lending itself to a periodic representation.

3.4.2 Functional Principal Component Regression

The model used for the FPCR is described in Estimation using Functional Principal Components. In addition to the selection of the truncation parameter L , the choice of the number of FPC's adds to the

complexity of the model since the approximated Eigenvalues and -functions from the decomposition are influenced by the choice of L that was used to expand the function. But since the FPCR is ultimately estimated with a linear model with the corresponding scores as regressors, the relevant degrees of freedom in the estimation of the ultimate model are not affected by L , but only by the number of FPC's $n_{FPC} \in \{2, 3, 4\}$. As will be described, it seems that neither a convex behavior of the MSPE nor any clear relationship can be observed between the number of basis functions and the number of FPC's. This might be because the dependency **Reformulate this in the meeting!!!** (FPCA is performed on the smoothed curves) is too complex to draw conclusions regarding this within this simulation study. Therefore, we will limit ourselves to a brief description. In this simulation, the cross-validated choice of basis functions indicates that the FPCR might not take the differing signal-to-noise ratios of the responses into account (same number of basis functions for the different signal-to-noise ratios). A possible explanation might be that the FPC's, which affect the relevant degrees of freedom, are solely calculated from the smoothed curves, not considering the noise in the responses.

Monomial Basis For f_1 , the cross-validated MSPE is decreasing in the number of FPC's and chosen basis functions for both the high and the low signal-to-noise ratio (4, 5, 6 basis functions for $n_{FPC} \in \{2, 3, 4\}$). In f_2 , we also observe a decreasing MSPE in the number of FPC's, but no clear relationship for the chosen basis functions. The Monomial basis shows the weakest performance for all three bases in each setting for all n_{FPC} .

B-spline Basis For f_1, Y_1 , the MSPE suggests that models with a higher number of FPC's perform better. While the number of basis functions stays at five for $n_{FPC} = 2, 3$, it increases to 6 basis functions for $n_{FPC} = 4$. In f_1, Y_2 , the cross-validated MSPE is only slightly affected by n_{FPC} , but lowest for $n_{FPC} = 3$, indicating the possibility of overfitting using $n_{FPC} = 4$. Similar to the two setups with f_1 , the cross-validated number of basis functions for f_2 is increasing in the number of FPC's (4, 6, 23 for $n_{FPC} \in \{2, 3, 4\}$)

Fourier Basis In f_1, Y_1 , the MSPE decreases in n_{FPC} while the results in f_1, Y_2 might indicate overfitting when using $n_{FPC} = 4$. f_2, Y_1 displays the greatest relative decline of MPSE in the increasing number of FPC's, but in absolute values, therefore acknowledging the higher noise responses for f_2, Y_2 , the decline of MSPE is similar to the decline observed for f_2, Y_2 . Both configurations of f_2 use 5, 15 and 7 basis functions for $n_{FPC} \in \{2, 3, 4\}$.

3.4.3 Interpretation and Relevance for Application

A possible explanation applicable to the setups performing Basis Expansion Regression might be the effect of the Bias-Variance tradeoff and the following hypothesis: For f_1 , only little bias seems to be introduced when choosing a small number of basis functions. For f_2 , a higher number of basis functions seems appropriate, resulting from the inherent peculiarities of f_2 that are more pronounced with higher L . This results in higher numbers of basis functions since the bias is decreasing faster than the variance is increasing in the number of basis functions compared to f_1 . The described convex behavior of the MSPE might also be partially attributable to the bias-variance tradeoff.

This convex behavior was not observed for the FPCR where no clear relationship between the basis functions and the number of FPC could be uncovered. A hypothesis for this is that the dependency between the truncation parameter L and the FPC's, which are calculated from L -truncated smoothed curves, is too complex to capture in our setting. To examine this further, additional simulations (

Appendix 6.4) were conducted for B-spline basis functions with a large truncation parameter $L \in \{50, 70\}$ for $n_{FPC} \in \{2, \dots, 7\}$. As in the simulation study, we can find potential signs of overfitting for all setups and both choices of L . The additional simulations revealed evidence that there might exist a relationship from $n_{FPC} = 3$ onwards: For $n_{FPC} \in \{3, \dots, 7\}$, the 10-fold cross-validated MSPE is always lower for 50 than for 70 basis functions which might be the first sign of an L that is chosen too large and subsequent undersmoothing. Following this, it seems that once a sufficient number of basis functions is used to expand the curves, the FPCR performs better using a more conservative number of basis functions (here $L = 50$). The settings f_1, Y_2 and f_2, Y_2 perform worse for these high number of basis functions compared to the main simulation, while f_1, Y_1 and f_2, Y_1 show a stronger performance than in the main simulation study, although the signal-to-noise ratios of the responses are not affecting the construction of the FPC's. This might indicate beneficial attributes of a lower truncation parameter in settings with low signal-to-noise responses.

4 Application

Our application uses the methods and insights from the previous sections to predict the octane ratings of the gasoline data set. Although the simulation study granted valuable insights into the different methods in our four different settings, it is not enough to determine the optimal method and choice of basis for the application since there is too much uncertainty involved. To point out some sources of uncertainty: First, differing from the simulation setup, we do not know the true coefficient function. Visual inspection of the estimated coefficient functions shown in Appendix 6.7 fuels the hypothesis the real coefficient function might be more similar to f_2 than to f_1 , but the insights from the two functions are not sufficient to draw any conclusion. Second, we have no information about the signal-to-noise ratio of the measured octane numbers. Third, to generate similar curves, we made assumptions about the distribution of ξ that are not applicable in this application where we do not know their distribution. Therefore, we will rerun all specifications for the gasoline data set and use the results of the simulation study to improve our understanding of the results. The application is designed analogously to the simulation study: The 60 spectra of the gasoline data set will be used to estimate a coefficient function, predict the reported octane numbers, and evaluate the results via MSPE using 12 fold cross-validation with 5 elements per fold. In total, we conducted 1000 repetitions for each setting.

4.1 Interpretation of Results

4.1.1 Basis Expansion Regression

The cross-validated MSPE selects 5 basis functions for the Monomial basis. For B-Splines, the cross-validation selects 10 basis functions and 9 basis functions for the Fourier basis. Comparing $\hat{\beta}(t)$ for the different bases in figure 25, away from the boundaries, the B-spline and Fourier bases show similar behavior, opposing to the Monomial estimate, which might be attributable to the lower number of basis functions. Especially at the lower boundary, the Monomial basis shows an exaggerated behavior. However, we must exercise caution since from $L = 6$ onwards, we could not calculate stable results for the Monomial basis. The MSPE for B-splines (0.04574) and Fourier (0.04808) are similar, while the Monomial basis (0.24181) shows distinctly worse properties. In contrast to the simulation study, the B-splines basis outperforms the Fourier basis. Driving factors for this improved performance could be that we do not assume a periodic coefficient function with the same start- and end value and second,

that the Fourier basis enforces identical start and end value on NIR. It is worthy to note that the reported MSPE for the B-spline and Fourier basis are close to the errors reported in the simulation study for the setup f_2, Y_1 , which might be caused by the hypothesized similarities between the actual coefficient function and f_2 , but also by a similar high signal-to-noise ratio of the octane numbers.

4.1.2 Functional Principal Component Regression

The best performance for all numbers of FPC's was achieved with the Fourier Basis, as for the FPCR in the simulation study. In contrast to the simulation study, no evidence of overfitting was found for the best basis choices in any of the three bases. The MSPE for the optimal specification appears to be strictly decreasing in the number of FPC's. As for the simulation study, the interpretation of the results with respect to the chosen basis is difficult: Referring to the plotted estimates $\hat{\beta}(t)$ in figure 26, 27 and 28, it appears to be the case that the higher n_{FPC} is, the more similar behavior of the estimate $\hat{\beta}(t)$ can be observed. Differing from the simulation study, the number of basis functions steadily increases for the Monomial basis. The behavior for the B-spline basis is similar to the one reported in the simulation study (basis functions increasing in n_{FPC}).

5 Outlook

Limitations

Insights from Simulation cannot be Extended to More General Functions As described, the properties of the two used functions $f \in \{f_1(t), f_2(t)\}$ influence the results. Although the resulting MSPE and visual inspection provided some evidence to support the hypothesis that the true coefficient function of *NIR* might be similar to f_2 , several other factors that were not asserted could also have caused this. Therefore, this simulation is not sufficient to base a reasonable claim concerning more general true coefficient functions, as we would assume them in other applications, on it.

Collinearity Problems in Basis Expansion Regression As already described in the section on the simulation study, the basis expansion regression was in part limited by the numerical instability of the estimation procedure. This is mainly due to an increase in collinearity of the derived regressor matrix shown in Definition 37. This problem is inherent to basis systems whose functions are not pairwise orthogonal, such as the Monomial or B-splines bases, but gets more pronounced the more functions we add to the basis system and the higher the correlation between those functions.

The numeric instability of the inversion of this matrix makes the estimates unreliable and therefore can make this approach infeasible for non-orthogonal bases in settings where the characteristics of the data set demand a higher number of basis functions than is feasible due to the properties of the estimation procedure.

Low Number of Basis Functions in FPCR Regression As the simulation and application showed, the number of basis functions does not seem to be the deciding factor for the performance of FPCR, apart from the additional simulations, which reported signs of undersmoothing for larger values of L . A more significant factor seems to be the number of FPC's available for the linear regression. This paper selects these components by their corresponding Eigenvalues. For reasons outlined in Section 3.1 it might be better to make the selection of the FPC's subject to some criteria such as cross-validation or base their choice on insights and expertise from the respective field.

Possible Extensions

Orthogonal Polynomials to Solve Collinearity Problems of Monomial Basis To address the collinearity problems described earlier, one possible idea would be to use a system of pair-wise orthogonal polynomials as a basis instead of the Monomial basis. One example is the system of Legendre polynomials which are orthogonal by construction and have the same closed span as the monomials (cf. Dattoli, Ricci, and Cesarano 2001). Due to their orthogonality, the problem of collinearity in the regressor matrix is greatly reduced, which could allow for larger numbers of basis functions in the basis expansion regression approach. The first eight Legendre polynomials are shown in Appendix section 6.2.

Comparison to Penalty Based Smoothing Procedures In contrast to the more typical approach of using a large but often arbitrary number of basis functions and smoothing using a penalty term involving, for example, the second derivative of the curve, this paper focuses on smoothing by using a smaller number of basis functions. As a next step to the analysis of this paper, it would be interesting to compare both methods to see in which settings different approaches to smoothing perform better and if a possible combination of both approaches could be advantageous.

Larger Range for the Number of Specifications for FPCR As alluded to before, the chosen specifications for the number of principal components and the number of basis functions used for FPCR might be insufficient to obtain a complete picture of the performance of this procedure when combined with smoothing using basis truncation. It would therefore be interesting to focus more attention on this limitation of this paper in a future extension to explore a broader array of possible specifications which might allow the derivation of more detailed insights.

Input from Physics It would be interesting to combine the purely mathematical findings of this paper with theoretical expertise from the field of physics, as this could inform the choice of models and be conducive to a more meaningful interpretation of estimates. For example, specific parts of the NIR spectrum can possibly be linked to specific molecules associated with high predictive power for the octane value. This could guide, for example, the construction of a B-spline basis that focuses on the relevant parts of the spectrum by using a vector of knots founded by field expertise. Alternatively, it could be used to link specific principal components to chemical compounds, which would be useful for the model selection and interesting for the interpretation of estimates.

6 Appendix

6.1 Near-infrared (NIR) Spectroscopy

NIR- spectroscopy is a spectroscopic method that uses the near-infrared region of the electromagnetic spectrum (From 780 nm to 2500 nm). It measures the absorption and interaction of this spectrum of radiation with the sample. NIR-spectroscopy is not only faster and cheaper than the standard test procedure – another significant advantage is that it does not need a reagent and thus does not destroy the sample. It is used for analysis in different sectors and fields, like the agrochemical industry and healthcare. Its non-invasive nature makes it also an asset for medical applications like the monitoring of diabetes in which NIR-spectroscopy can detect the worsening of the blood glucose metabolic dysfunction (cf . Li et al. 2020).

In the context of this paper, the gasoline data set which is used for the simulation and the application is constructed using NIR spectroscopy. According to Gy. Bohács, Z. Ovádi, A. Salgó 1998 NIR-spectroscopy is a feasible method for the analysis of gasoline since most of the absorption that is observed within the described interval of wavelengths is due to overtones and interactions of the radiation with chemical combinations (carbon–hydrogen, carbon–carbon, carbon–oxygen, carbonyl associated groups, aromatic stretching, and deformation vibration of the hydrocarbon molecules). While this paper focuses on the prediction of the octane number of gasoline, other research focuses on different properties of gasoline such as the olefin, naphthaenic and aromatic content (Parisi et al. 1990, as cited in Gy. Bohács, Z. Ovádi, A. Salgó 1998) or the distillation characteristics (Pauls 1985, as cited in Gy. Bohács, Z. Ovádi, A. Salgó 1998)



Figure 4: NIR absorption spectra from the Gasoline Data Set and Finder SD (a Near-Infrared-Spectroscope built by HiperScan GmbH)

(Source: https://www.hiperscan.com/files/apoident/uploads/Bilder/Neue_Website/Produkte/FinderSD.jpg)

6.2 Basis Plots



Figure 5: Fourier basis functions for $i = 1, \dots, 7$



Figure 6: B-spline basis functions of order 4 for 8 equidistant knots on $[0, 1]$



Figure 7: Monomial basis functions of degree 0 to 7

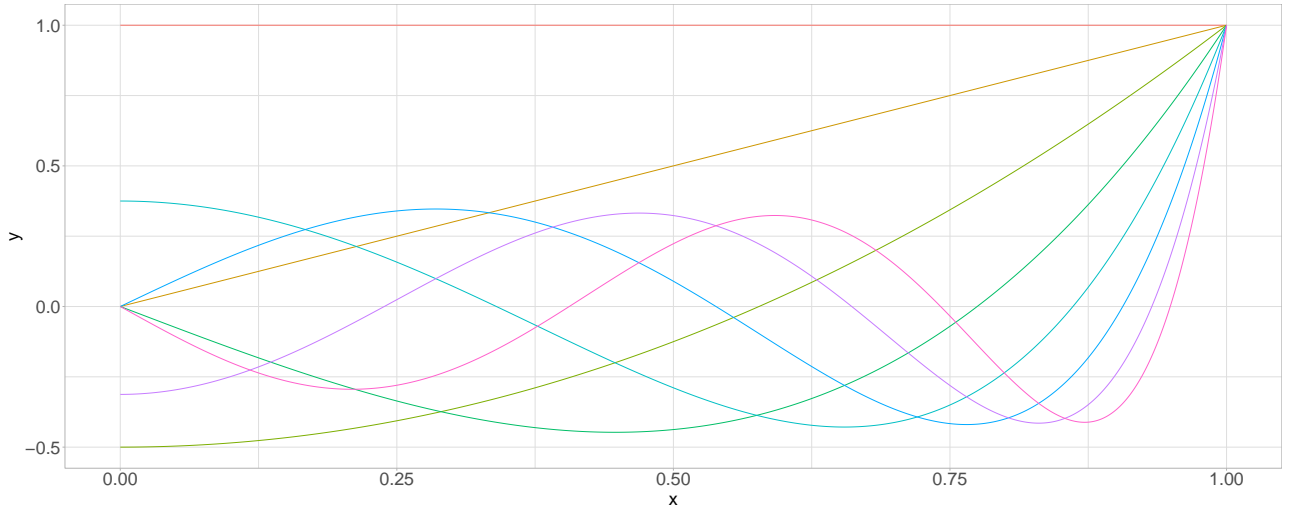


Figure 8: Legendre Polynomials of degree 0 to 7

6.3 Simulation Study Results

Table 1: Monomial Basis Expansion Regression

f_1, Y_1	f_1, Y_2	f_2, Y_1	f_2, Y_2	n_basis
7.17723	131.92717	0.89367	2.58395	2
4.17039	129.64259	0.81224	2.51177	3
3.91275	130.11708	0.38079	2.09047	4
3.6385	130.59817	0.09217	1.81343	5
6.01644	201.15535	0.76208	3.39373	6

Table 2: B-Spline Basis Expansion Regression

f_1, Y_1	f_1, Y_2	f_2, Y_1	f_2, Y_2	n_basis
3.91275	130.11708	0.38079	2.09047	4
3.64305	130.61095	0.09512	1.81643	5
3.65426	131.35355	0.07775	1.80913	6
3.67705	132.14205	0.07518	1.8168	7
3.71074	133.36537	0.0581	1.8165	8
3.71921	133.68149	0.0564	1.81931	9
3.74201	134.51217	0.05218	1.82576	10
3.7644	135.29727	0.0519	1.8361	11
3.80109	136.57581	0.05204	1.85315	12
3.83436	137.78407	0.05271	1.86997	13
3.86217	138.73431	0.05307	1.88269	14
3.86856	138.97427	0.0526	1.88482	15
3.88506	139.57419	0.05283	1.89335	16
3.91267	140.5149	0.05322	1.90619	17
3.94813	141.80885	0.05358	1.92312	18

Table 3: Fourier Basis Expansion Regression

f_1, Y_1	f_1, Y_2	f_2, Y_1	f_2, Y_2	n_basis
3.69752	129.19134	0.69524	2.3944	3
3.6347	130.59282	0.07418	1.79582	5
3.67623	132.08248	0.05147	1.79343	7
3.71885	133.67575	0.05105	1.81291	9
3.76451	135.26219	0.05146	1.83463	11
3.81095	136.90282	0.05197	1.85724	13
3.85674	138.57258	0.05252	1.88021	15
3.90619	140.29178	0.05304	1.90283	17
3.95517	142.05727	0.05365	1.92718	19

Table 4: Monomial FPCR, $nharm = 2$

f_1, Y_1	f_1, Y_2	f_2, Y_1	f_2, Y_2	n_basis
7.17723	131.92717	0.89367	2.58395	2
5.89626	130.64918	0.81105	2.50111	3
5.807	130.55792	0.77154	2.46164	4
6.07681	130.82169	0.77836	2.4684	5
6.55003	131.28414	0.77506	2.465	6
7.55111	132.26672	0.73771	2.42761	7
11.62846	136.28281	0.74403	2.43402	8
17.29836	141.88633	0.69837	2.38887	9
18.84999	143.43309	0.64904	2.33978	10
18.88329	143.46571	0.69403	2.38461	11
18.99159	143.63082	0.81692	2.50713	12

Table 5: Monomial FPCR, $nharm = 3$

f_1, Y_1	f_1, Y_2	f_2, Y_1	f_2, Y_2	n_basis
4.17039	129.64259	0.81224	2.51177	3
4.08093	129.55048	0.77174	2.47128	4
4.0038	129.49674	0.75004	2.44986	5
4.17563	129.68591	0.45954	2.1605	6
4.23226	129.74146	0.52512	2.226	7
4.4198	129.91964	0.74368	2.4439	8
4.42156	129.92039	0.69479	2.39518	9
4.4125	129.91256	0.64087	2.34145	10
4.44546	129.94476	0.6792	2.37965	11
11.82311	137.32413	0.74329	2.44296	12

Table 6: Monomial FPCR, $nharm = 4$

f_1, Y_1	f_1, Y_2	f_2, Y_1	f_2, Y_2	n_basis
3.91274	130.1171	0.38077	2.09045	4
3.95242	130.16289	0.73944	2.44922	5
3.8366	130.05179	0.27201	1.98372	6
3.96405	130.17512	0.30729	2.01904	7
4.38618	130.61211	0.11108	1.82326	8
4.44028	130.66082	0.13501	1.84706	9
4.4251	130.64453	0.1455	1.85748	10
4.44727	130.66669	0.14012	1.85223	11
7.88834	134.08085	0.17742	1.8879	12

Table 7: B-Spline FPCR, $nharm = 2$

f_1, Y_1	f_1, Y_2	f_2, Y_1	f_2, Y_2	n_basis
10.93556	135.66335	0.69614	2.38597	4
6.01366	130.75986	0.77796	2.46801	5
6.36762	131.10562	0.79035	2.48029	6
6.76471	131.49507	0.7684	2.45834	7
7.21393	131.93622	0.7958	2.48568	8
7.77885	132.48984	0.75447	2.44437	9
8.48517	133.18046	0.71664	2.40654	10
8.95142	133.63714	0.70481	2.39475	11
9.21314	133.89421	0.71456	2.4045	12
9.29854	133.97794	0.73961	2.42952	13
9.31792	133.99732	0.74046	2.43037	14
9.32858	134.00809	0.74354	2.43344	15
9.27722	133.95811	0.77399	2.46383	16
9.23813	133.91976	0.77175	2.46159	17
9.33983	134.01705	0.76653	2.45632	18
9.24067	133.92097	0.78389	2.47367	19
9.34246	134.01837	0.75304	2.44285	20
9.38735	134.06288	0.76148	2.45127	21
9.35218	134.02839	0.75842	2.44823	22
9.50715	134.17875	0.74067	2.43049	23
9.51344	134.18666	0.7552	2.44502	24
9.52277	134.19463	0.75125	2.44107	25

Table 8: B-Spline FPCR, $nharm = 3$

f_1, Y_1	f_1, Y_2	f_2, Y_1	f_2, Y_2	n_basis
4.26915	129.73814	0.65618	2.35517	4
3.99153	129.47951	0.75902	2.45877	5
4.13265	129.64227	0.42504	2.126	6
4.15027	129.66158	0.52603	2.22684	7
4.28266	129.7862	0.71107	2.41134	8
4.30464	129.8084	0.65968	2.36019	9
4.32579	129.82882	0.60062	2.3013	10
4.29797	129.80089	0.65658	2.35703	11
4.32782	129.82922	0.68072	2.38108	12
4.34042	129.84041	0.71583	2.41605	13
4.3526	129.8512	0.72262	2.42279	14
4.3577	129.85642	0.72621	2.42637	15
4.37694	129.87493	0.75746	2.45749	16
4.35973	129.85893	0.75291	2.45296	17
4.37223	129.87141	0.69875	2.39878	18
4.34433	129.84395	0.74346	2.44353	19
4.36545	129.86595	0.67405	2.37412	20
4.36942	129.86886	0.67941	2.37944	21
4.34272	129.843	0.6919	2.39205	22
4.38437	129.88403	0.64702	2.34708	23
4.35012	129.8495	0.68435	2.38446	24
4.36866	129.86795	0.67512	2.37514	25

Table 9: B-Spline FPCR, $nharm = 4$

f_1, Y_1	f_1, Y_2	f_2, Y_1	f_2, Y_2	n_basis
3.91274	130.1171	0.38077	2.09045	4
3.97061	130.18108	0.75664	2.46627	5
3.83646	130.05682	0.19244	1.90433	6
3.8814	130.0934	0.3326	2.04419	7
4.2679	130.49905	0.09497	1.8071	8
4.31978	130.54252	0.15828	1.87039	9
4.32413	130.5527	0.10538	1.81745	10
4.31263	130.53896	0.13116	1.84322	11
4.33997	130.56608	0.10762	1.81971	12
4.34107	130.56642	0.11868	1.83076	13
4.35627	130.57893	0.12832	1.84037	14
4.35369	130.57747	0.11173	1.82379	15
4.35313	130.57695	0.11652	1.82861	16
4.3476	130.57119	0.11283	1.82497	17
4.31541	130.54208	0.08832	1.80044	18
4.32121	130.54666	0.10087	1.81304	19
4.2968	130.52361	0.08341	1.79552	20
4.30044	130.52787	0.08785	1.79994	21
4.29859	130.52514	0.08833	1.80045	22
4.28391	130.51071	0.08189	1.79394	23
4.29418	130.52054	0.08928	1.80134	24
4.28911	130.51512	0.0856	1.79766	25

Table 10: Fourier FPCR, $nharm = 2$

f_1, Y_1	f_1, Y_2	f_2, Y_1	f_2, Y_2	n_basis
5.04859	129.81003	0.78889	2.4789	3
5.08647	129.84459	0.69756	2.38778	5
5.29235	130.04946	0.80393	2.49395	7
5.32414	130.07859	0.80074	2.49072	9
5.34403	130.09777	0.79714	2.48713	11
5.43601	130.18816	0.8141	2.50404	13
5.51333	130.26036	0.78908	2.47902	15
5.70153	130.44275	0.79659	2.48646	17
5.87259	130.6101	0.77783	2.46771	19

Table 11: Fourier FPCR, $nharm = 3$

f_1, Y_1	f_1, Y_2	f_2, Y_1	f_2, Y_2	n_basis
3.69752	129.19134	0.69524	2.3944	3
5.06895	130.54881	0.1376	1.83947	5
5.21758	130.69839	0.13994	1.84156	7
5.22636	130.70697	0.12715	1.82896	9
5.27531	130.74943	0.14282	1.84453	11
5.29036	130.76091	0.13007	1.83175	13
5.16722	130.64051	0.10365	1.80524	15
4.98841	130.46747	0.11563	1.81733	17
4.92246	130.40322	0.14766	1.84937	19

Table 12: Fourier FPCR, $nharm = 4$

f_1, Y_1	f_1, Y_2	f_2, Y_1	f_2, Y_2	n_basis
3.61833	129.83284	0.07736	1.78876	5
3.66209	129.88835	0.06311	1.77442	7
3.68812	129.91351	0.0717	1.78321	9
4.10715	130.34635	0.08317	1.79518	11
4.17569	130.4147	0.08837	1.80046	13
4.21112	130.44645	0.09965	1.81164	15
4.2129	130.45091	0.08775	1.79975	17
4.21884	130.45501	0.09032	1.80229	19

6.4 Additional Simulation

Table 13: Additional Runs B-Splines for $L \in \{50, 70\}$

n_FPC	f_1, Y_1	f_1, Y_2	f_2, Y_1	f_2, Y_2	n_basis
2	12.01215	136.37917	0.74396	2.45234	50
2	12.63307	136.79449	0.73227	2.43754	70
3	4.98379	130.27154	0.62033	2.33437	50
3	6.70572	131.58072	0.69647	2.40584	70
4	4.33014	130.23059	0.08985	1.81309	50
4	5.81452	131.05453	0.26875	1.9835	70
5	4.07164	130.68035	0.06323	1.79676	50
5	5.083	131.08668	0.22106	1.94707	70
6	3.70117	131.04066	0.06245	1.80571	50
6	5.62771	132.62722	0.23593	1.97606	70
7	3.69911	131.80298	0.05566	1.8068	50
7	5.37466	133.80644	0.27455	2.03417	70

6.5 Simulation - Coefficient Function Estimates

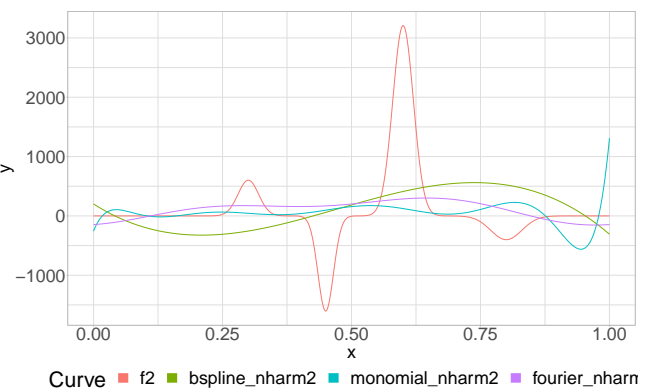
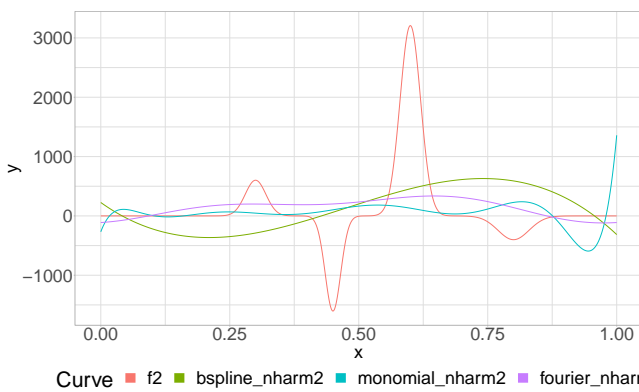
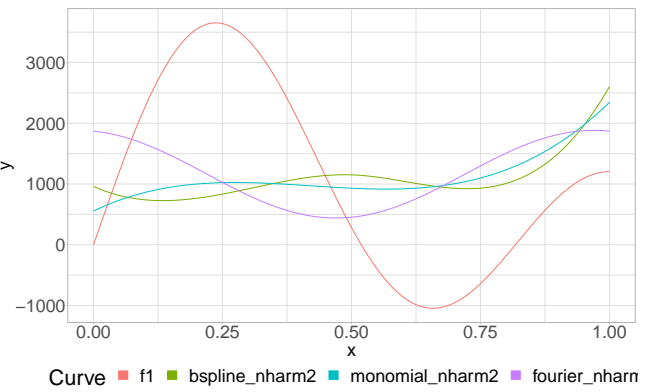
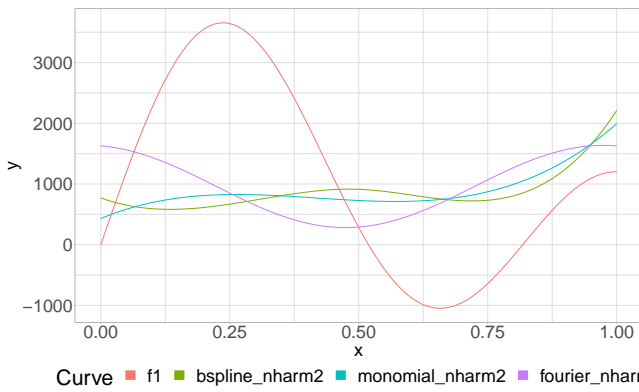
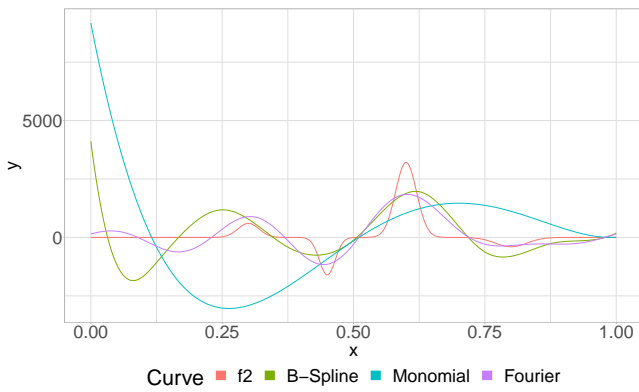
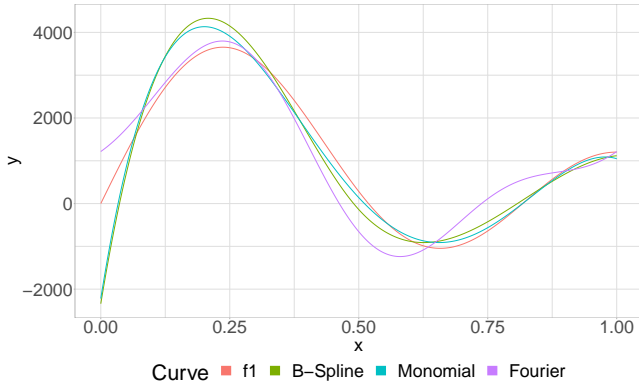




Figure 17: FPC Regression, 3 harmonics - f_1, Y_1

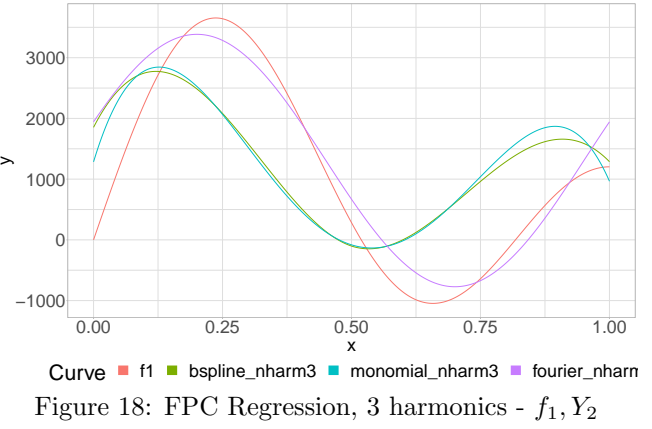


Figure 18: FPC Regression, 3 harmonics - f_1, Y_2

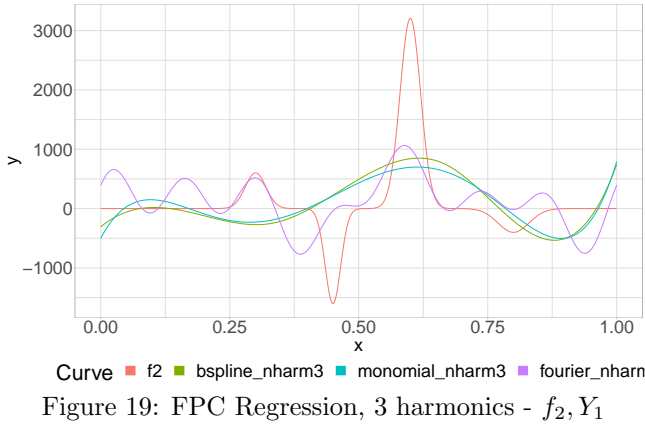


Figure 19: FPC Regression, 3 harmonics - f_2, Y_1

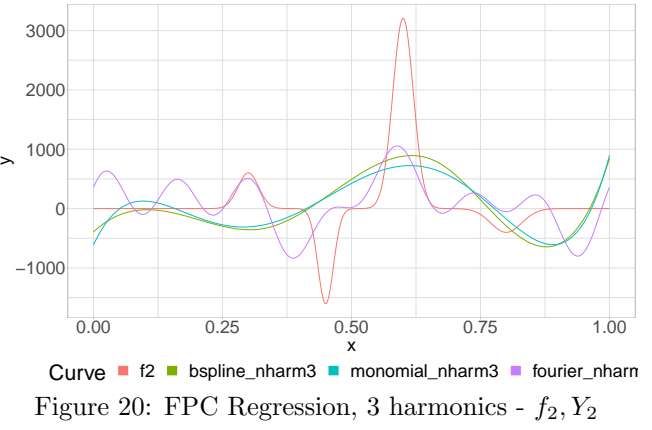


Figure 20: FPC Regression, 3 harmonics - f_2, Y_2

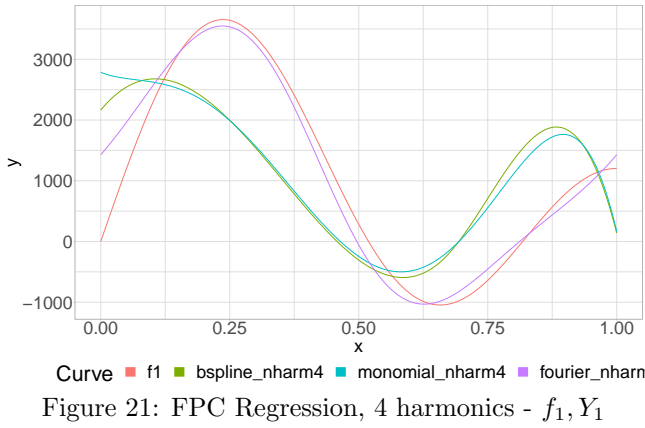


Figure 21: FPC Regression, 4 harmonics - f_1, Y_1

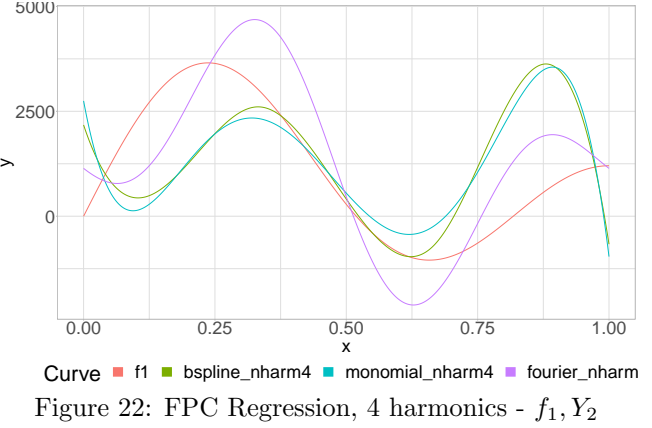


Figure 22: FPC Regression, 4 harmonics - f_1, Y_2

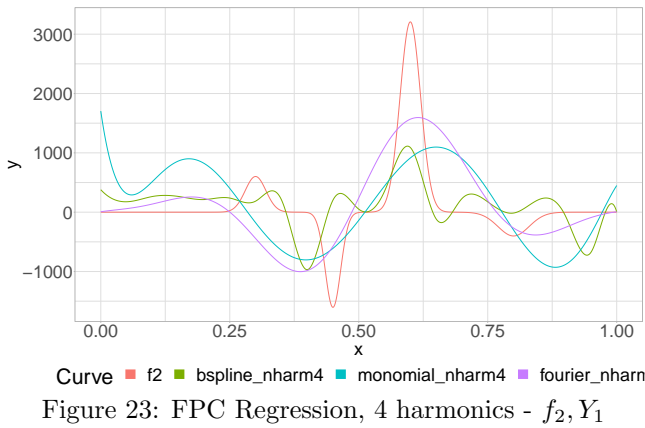


Figure 23: FPC Regression, 4 harmonics - f_2, Y_1

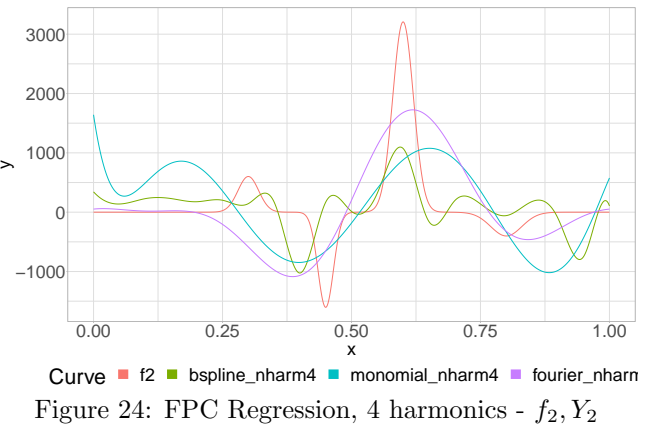


Figure 24: FPC Regression, 4 harmonics - f_2, Y_2

6.6 Application Results

Table 14: Application Results Basis Expansion Regression

Monomial	B-Spline	Fourier	n_basis	fold_size	n_folds
2.29641			2	5	12
2.11258		2.07767	3	5	12
0.73444	0.73444		4	5	12
0.24181	0.2544	0.07430	5	5	12
8.88013	0.08621		6	5	12
	0.11177	0.05021	7	5	12
	0.05012		8	5	12
	0.07465	0.04808	9	5	12
	0.04574		10	5	12
	0.05629	0.05456	11	5	12
	0.05291		12	5	12
	0.06083	0.05558	13	5	12
	0.06926		14	5	12
	0.09058	0.07920	15	5	12
			16	5	12
		0.06161	17	5	12
			18	5	12
		0.10976	19	5	12

Table 15: Application Results Monomial FPCR

2 FPC	3 FPC	4 FPC	n_basis	fold_size	n_folds
2.29642			2	5	12
2.17648	2.11259		3	5	12
2.21978	2.17702	0.73432	4	5	12
2.21854	2.23061	2.35328	5	5	12
2.21896	1.98803	0.84386	6	5	12
2.23156	2.07872	0.85358	7	5	12
2.19982	2.25104	0.11363	8	5	12
2.24343	2.21964	0.11476	9	5	12
2.18792	2.11694	0.12084	10	5	12
2.20919	2.15677	0.08986	11	5	12
2.27197	2.21142	0.14176	12	5	12

Table 16: Application Results B-spline FPCR

2 FPC	3 FPC	4 FPC	n_basis	fold_size	n_folds
2.24364	2.1	0.73432	4	5	12
2.21916	2.21024	2.35745	5	5	12
2.2088	1.92703	0.55305	6	5	12
2.22042	2.10322	1.03165	7	5	12
2.17938	2.24933	0.076	8	5	12
2.20726	2.20003	0.18801	9	5	12
2.23642	2.08957	0.05669	10	5	12
2.23069	2.13131	0.09795	11	5	12
2.22878	2.14135	0.05523	12	5	12
2.1994	2.13177	0.06089	13	5	12
2.20168	2.14603	0.07197	14	5	12
2.20372	2.14908	0.05159	15	5	12
2.16851	2.13255	0.05724	16	5	12
2.17341	2.12780	0.06545	17	5	12
2.18263	2.00428	0.05399	18	5	12
2.15647	2.05871	0.06774	19	5	12
2.19268	1.96472	0.05542	20	5	12
2.17718	1.95345	0.0595	21	5	12
2.1798	1.99118	0.05519	22	5	12
2.1966	1.90692	0.05318	23	5	12
2.1786	1.97124	0.05725	24	5	12
2.18768	1.95758	0.0508	25	5	12

Table 17: Application Results Fourier FPCR

2 FPC	3 FPC	4 FPC	n_basis	fold_size	n_folds
2.13234	2.07788		3	5	12
2.26267	0.21409	0.19585	5	5	12
2.15572	0.06414	0.0435	7	5	12
2.16344	0.05448	0.05256	9	5	12
2.16087	0.06795	0.05276	11	5	12
2.13984	0.05848	0.05154	13	5	12
2.17941	0.14014	0.06486	15	5	12
2.16465	0.28983	0.05143	17	5	12
2.18426	0.43575	0.05255	19	5	12

6.7 Application - Coefficient Function Estimates

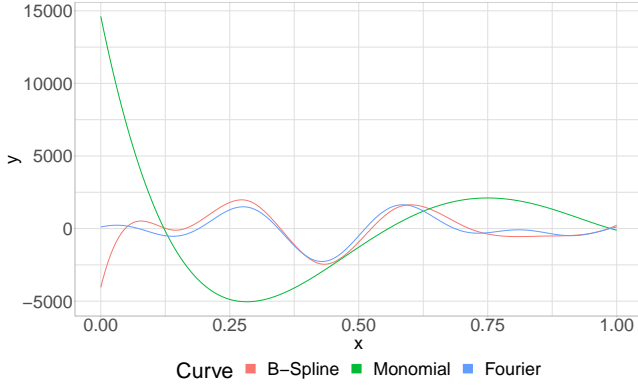


Figure 25: Basis Expansion Regression

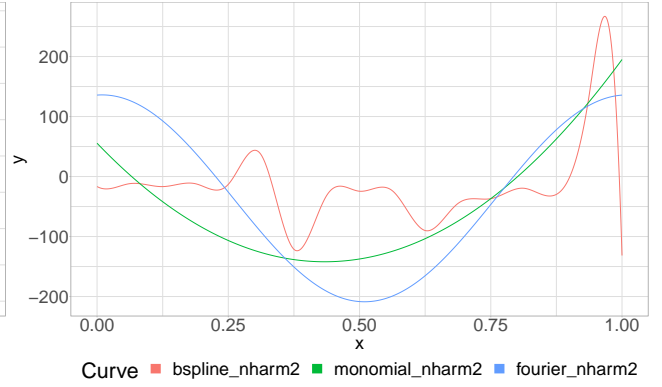


Figure 26: 2 Functional Principal Components

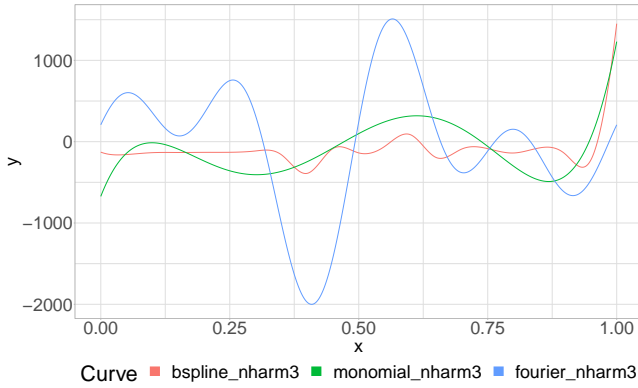


Figure 27: 3 Functional Principal Components

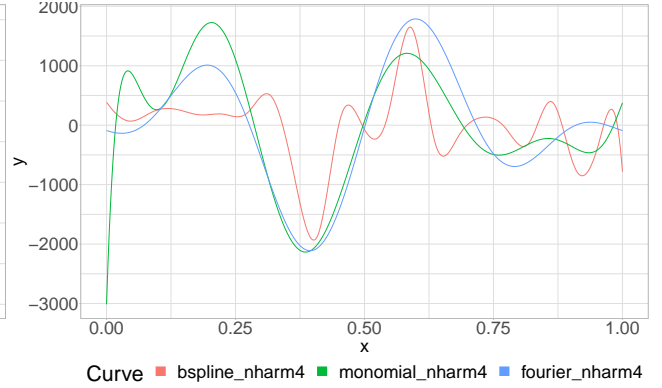


Figure 28: 4 Functional Principal Components

7 Definitions and Proofs

Alexanderian 2015 was referred for the following definitions and proofs.

7.1 Definition (Hilbert-Schmidt Integral Operator)

Given a bounded domain $\mathcal{A} \subset \mathbb{R}^n$, we call a function $c : \mathcal{A} \times \mathcal{A} \rightarrow \mathbb{R}$ a Hilbert-Schmidt kernel if

$$\int_{\mathcal{A}} \int_{\mathcal{A}} |c(x, y)|^2 dx dy < \infty \quad (55)$$

where $c \in \mathbb{L}^2(\mathcal{A} \times \mathcal{A})$. Let K be an integral operator on $\mathbb{L}^2(\mathcal{A})$ such that $K : \nu \rightarrow K\nu$ for $\nu \in \mathbb{L}^2(\mathcal{A})$, by

$$[K\nu](x) = \int_{\mathcal{A}} c(x, y)\nu(y)dy \quad (56)$$

When an integral operator K is linear and bounded, it is called a Hilbert-Schmidt operator. The linearity of the operator K is simply proved. Additionally assume that $\alpha, \beta \in \mathbb{R}$ and $\theta \in \mathbb{L}^2(\mathcal{A})$.

$$\begin{aligned}
[K(\alpha\nu + \beta\theta)](x) &= \int_{\mathcal{A}} c(x, y)(\alpha\nu(y) + \beta\theta(y))dy \\
&= \int_{\mathcal{A}} c(x, y)\alpha\nu(y)dy + \int_{\mathcal{A}} c(x, y)\beta\theta(y)dy \\
&= \alpha \int_{\mathcal{A}} c(x, y)\nu(y)dy + \beta \int_{\mathcal{A}} c(x, y)\theta(y)dy \\
&= \alpha[K\nu](x) + \beta[K\theta](x)
\end{aligned} \tag{57}$$

For boundedness of the oprator K ,

$$\begin{aligned}
\|K\nu\|_{\mathbb{L}^2(\mathcal{A})}^2 &= \int_{\mathcal{A}} \left| [K\nu](x) \right|^2 dx \\
&= \int_{\mathcal{A}} \left| \int_{\mathcal{A}} c(x, y)\nu(y)dy \right|^2 dx \\
&\leq \int_{\mathcal{A}} \left(\int_{\mathcal{A}} |c(x, y)|^2 dy \right) \left(\int_{\mathcal{A}} |\nu(y)|^2 dy \right) dx \quad (\text{Cauchy-Schwarz}) \\
&= \|c\|_{\mathbb{L}^2(\mathcal{A} \times \mathcal{A})} \|\nu\|_{\mathbb{L}^2} < \infty
\end{aligned} \tag{58}$$

7.2 Lemma

The curves $X(t) \in \mathbb{L}^2[0, 1]$ is expanded by the Eigenfunctions $\{\nu^m\}$ as Equation 18. The coefficients ξ^m corresponding to Eigenfunctions ν^m satisfy the following properties:

1. $\mathbb{E}[\xi^m(\omega)] = 0$
2. $Cov(\xi^m(\omega), \xi^n(\omega)) = \delta^{m,n} \lambda^m$
3. $Var(\xi^m(\omega)) = \lambda^m$

Remind that $\delta^{m,n} = 0$ if $m \neq n$, otherwise 1.

Proof. Assume that $F(t)$ is the centered process of $X(t)$, namely, $F(t) = X(t) - \int_{\Omega} X(t)dP(\omega)$. To obtain the first result, we can show that

$$\begin{aligned}
\mathbb{E}[\xi^m] &= \mathbb{E} \left[\int_0^1 F(t) \nu_j(t) dt \right] \\
&= \int_{\Omega} \int_0^1 F(t) \nu^m(t) dt dP(\omega) \\
&= \int_0^1 \int_{\Omega} F(t) \nu^m(t) dP(\omega) dt \quad (\text{Fubini}) \\
&= \int_0^1 \int_{\Omega} F(t) dP(\omega) \nu^m(t) dt \\
&= \int_0^1 \mathbb{E}[F(t)] \nu^m(t) dt = 0
\end{aligned} \tag{59}$$

where $\mathbb{E}[F(t)]$ is 0 since $F(t)$ is a centered process. The second claim is proved as:

$$\begin{aligned}
\mathbb{E}[\xi^m \xi^n] &= \mathbb{E} \left[\int_0^1 F(s) \nu^m(s) ds \int_0^1 F(t) \nu^n(t) dt \right] \\
&= \mathbb{E} \left[\int_0^1 \int_0^1 F(s) \nu^m(s) F(t) \nu^n(t) ds dt \right] \quad (\text{Fubini}) \\
&= \int_0^1 \int_0^1 \mathbb{E}[F(s) F(t)] \nu^m(s) \nu^n(t) ds dt \\
&= \int_0^1 \left(\int_0^1 c(s, t) \nu^m(s) ds \right) \nu^n(t) dt \\
&= \int_0^1 [K \nu^m](t) \nu^n(t) dt \\
&= \langle K \nu^m, \nu^n \rangle \\
&= \langle \lambda^m \nu^m, \nu^n \rangle = \delta^{m,n} \lambda^m
\end{aligned} \tag{60}$$

where $\delta^{m,n} = 1$ if $m = n$, otherwise 0. The result is produced from orthonormality of the Eigenfunctions.

$$Cov(\xi^m, \xi^n) = \mathbb{E}[\xi^m \xi^n] - \mathbb{E}[\xi^m] \mathbb{E}[\xi^n] = \delta^{m,n} \lambda^m \tag{61}$$

where $\mathbb{E}[\xi^m] = \mathbb{E}[\xi^n] = 0$ as the first property. The last assertion is confirmed from the above two properties.

$$Var[\xi^m] = \mathbb{E}[(\xi^m - \mathbb{E}[\xi^m])^2] = \mathbb{E}[(\xi^m)^2] = \lambda^m \tag{62}$$

The original process $X(t)$ also has the same properties as the centered one since

$$X(t) = F(t) + \mathbb{E}[X(t)] = \mu(t) + \sum_{m=1}^{\infty} \xi^m \nu^m(t) \tag{63}$$

□

7.3 Theorem (Karhunen-Lo  ve Expansion)

Let $X : [0, 1] \rightarrow \mathbb{R}$ be a mean-square continuous stochastic process, namely, $\lim_{\epsilon \rightarrow 0} \mathbb{E}[(X(t + \epsilon) - X(t))^2] = 0$, such that $X \in \mathbb{L}^2[0, 1]$. Then there exists a basis ξ^m of $\mathbb{L}^2[0, 1]$ such that for all $t \in [0, 1]$,

$$X(t) = \mu(t) + \sum_{m=1}^{\infty} \xi^m \nu^m(t), \tag{64}$$

where $\mu(t)$ is the mean function of $X(t)$ and coefficients ξ^m are given by $\int_0^1 (X(t) - \mu(t)) \nu^m(t) dt$. These coefficients satisfy the following conditions.

1. $\mathbb{E}[\xi^m(\omega)] = 0$
2. $Cov(\xi^m(\omega), \xi^n(\omega)) = \delta^{m,n} \lambda^m$
3. $Var(\xi^m(\omega)) = \lambda^m$

Proof. Let K be a Hilbert-Schmidt operator as in Equation 17. We know that K has a complete set of Eigenfunctions ν^m in $\mathbb{L}^2[0, 1]$ and non-negative Eigenvalues λ^m since K is a positive compact

self-adjoint operator. With the reminder that ξ^m satisfy the three conclusions by Lemma 7.2, we prove this expansion by considering

$$\epsilon_N(t) := \mathbb{E} \left[\left(X(t) - \mu(t) - \sum_{m=1}^N \xi^m \nu^m(t) \right)^2 \right] = \mathbb{E} \left[\left(F(t) - \sum_{m=1}^N \xi^m \nu^m(t) \right)^2 \right] \quad (65)$$

where $F(t)$ is the centered process of $X(t)$. Once it is shown that $\lim_{N \rightarrow \infty} \epsilon_N(t) = 0$ uniformly in $[0,1]$, the proof is completed.

$$\begin{aligned} \epsilon_N(t) &= \mathbb{E} \left[\left(F(t) - \sum_{m=1}^N \xi^m \nu^m(t) \right)^2 \right] \\ &= \mathbb{E}[F(t)^2] - 2\mathbb{E} \left[F(t) \sum_{m=1}^N \xi^m \nu^m(t) \right] + \mathbb{E} \left[\sum_{m=1}^N \sum_{n=1}^N \xi^m \xi^n \nu^m(t) \nu^n(t) \right] \end{aligned} \quad (66)$$

Here, $\mathbb{E}[F(t)^2] = c(t, t)$ as in Equation 16 since $F(t)$ is the centered process. Now, take the second term

$$\begin{aligned} \mathbb{E} \left[F(t) \sum_{m=1}^N \xi^m \nu^m(t) \right] &= \mathbb{E} \left[F(t) \sum_{m=1}^N \left(\int_0^1 F(s) \nu^m(s) ds \right) \nu^m(t) \right] \\ &= \mathbb{E} \left[\sum_{m=1}^N \left(\int_0^1 F(t) F(s) \nu^m(s) ds \right) \nu^m(t) \right] \\ &= \sum_{m=1}^N \left(\int_0^1 \mathbb{E}[F(t) F(s)] \nu^m(s) ds \right) \nu^m(t) \\ &= \sum_{m=1}^N \left(\int_0^1 c(t, s) \nu^m(s) ds \right) \nu^m(t) \\ &= \sum_{m=1}^N [K \nu^m](t) \nu^m(t) \\ &= \sum_{m=1}^N \lambda^m \nu^m(t) \nu^m(t) = \sum_{m=1}^N \lambda^m \nu^m(t)^2 \end{aligned} \quad (67)$$

where the covariance function $c(t, s)$ has the Hilbert-Schmidt operator as in Equation 17. It turns out the product of the Eigenfunction and the corresponding Eigenvalue. For the last term, we derive from Equation 60 that

$$\begin{aligned} \mathbb{E} \left[\sum_{m=1}^N \sum_{n=1}^N \xi^m \xi^n \nu^m(t) \nu^n(t) \right] &= \sum_{m=1}^N \sum_{n=1}^N \mathbb{E}[\xi^m \xi^n] \nu^m(t) \nu^n(t) \\ &= \sum_{m=1}^N \sum_{n=1}^N \delta^{m,n} \lambda^m \nu^m(t) \nu^n(t) = \sum_{m=1}^N \lambda^m \nu^m(t)^2 \end{aligned} \quad (68)$$

where $\delta_{m,n} = 1$ if $m = n$, otherwise 0. Therefore, by Equations 66, 67, and 68 we obtain

$$\epsilon_N(t) = c(t, t) - \sum_{m=1}^N \lambda^m \nu^m(t) \nu^m(t) \quad (69)$$

implementing Mercer's Theorem this proof is concluded by

$$\lim_{N \rightarrow \infty} \epsilon_N(t) = \lim_{n \rightarrow \infty} \mathbb{E} \left[\left(F(t) - \sum_{m=1}^N \xi^m \nu^m(t) \right)^2 \right] = 0 \quad (70)$$

□

8 Bibliography

- Alexanderian, Alen (2015). “A brief note on the Karhunen-Loève expansion”. In: *arXiv: Probability*. URL: <https://arxiv.org/abs/1509.07526>.
- Bauer, Heinz (May 2020). *Wahrscheinlichkeitstheorie und Grundzüge der Maßtheorie*. de. De Gruyter. ISBN: 978-3-11-231316-9. DOI: 10.1515/9783112313169.
- Boor, Carl de (Jan. 1978). *A Practical Guide to Spline*. Vol. Volume 27. Journal Abbreviation: Applied Mathematical Sciences, New York: Springer, 1978 Publication Title: Applied Mathematical Sciences, New York: Springer, 1978. DOI: 10.2307/2006241.
- Cai, T. Tony and Peter Hall (Oct. 2006). “Prediction in functional linear regression”. In: *The Annals of Statistics* 34.5. Publisher: Institute of Mathematical Statistics, pp. 2159–2179. DOI: 10.1214/009053606000000830.
- Cardot, Hervé (2002). “Spatially Adaptive Splines for Statistical Linear Inverse Problems”. In: *Journal of Multivariate Analysis* 81.1, pp. 100–119. DOI: <https://doi.org/10.1006/jmva.2001.1994>.
- Dattoli, Giuseppe, Paolo Ricci, and Clemente Cesarano (Jan. 2001). “A Note on Legendre Polynomials”. In: *International Journal of Nonlinear Sciences and Numerical Simulation* 2. DOI: 10.1515/IJNSNS.2001.2.4.365.
- Goldsmith, Jeff et al. (2011). “Penalized Functional Regression”. In: *Journal of computational and graphical statistics : a joint publication of American Statistical Association, Institute of Mathematical Statistics, Interface Foundation of North America* 20.4, pp. 830–851. DOI: 10.1198/jcgs.2010.10007.
- Gy. Bohács, Z. Ovádi, A. Salgó (1998). “Prediction of Gasoline Properties with near Infrared Spectroscopy”. In: *Journal of near infrared spectroscopy*. 6, pp. 341–348.
- Horváth, Lajos and Piotr Kokoszka (May 2012). *Inference for Functional Data with Applications*. en. Springer Science & Business Media. ISBN: 978-1-4614-3655-3.
- Hsing, Tailen and Randall Eubank (Mar. 2015). *Theoretical Foundations of Functional Data Analysis, with an Introduction to Linear Operators*. en. John Wiley & Sons. ISBN: 978-1-118-76256-1.
- James, Gareth M., Jing Wang, and Ji Zhu (2009). “Functional linear regression that’s interpretable”. In: *The Annals of Statistics* 37.5A. DOI: 10.1214/08-AOS641.
- Jolliffe, Ian T. (1982). “A Note on the Use of Principal Components in Regression”. In: *Journal of the Royal Statistical Society: Series C (Applied Statistics)* 31.3, pp. 300–303. DOI: 10.2307/2348005.
- Kokoszka, Piotr and Matthew Reimherr (Aug. 2017). *Introduction to Functional Data Analysis*. Englisch. 1st ed. Boca Raton: Chapman and Hall/CRC. ISBN: 978-1-4987-4634-2.
- Levitin, Daniel et al. (Aug. 2007). “Introduction to Functional Data Analysis”. In: *Canadian Psychology/Psychologie canadienne* 48, pp. 135–155. DOI: 10.1037/cp2007014.
- Li, Yuanpeng et al. (2020). “Early Diagnosis of Type 2 Diabetes Based on Near-Infrared Spectroscopy Combined With Machine Learning and Aquaphotomics”. In: *Frontiers in Chemistry* 8, p. 1133. DOI: 10.3389/fchem.2020.580489.
- Ramsay, James and B. W. Silverman (2005). *Functional Data Analysis*. en. 2nd ed. Springer Series in Statistics. New York: Springer-Verlag. ISBN: 978-0-387-40080-8. DOI: 10.1007/b98888.
- Reiss, Philip T. and R. Todd Ogden (2007). “Functional Principal Component Regression and Functional Partial Least Squares”. In: *Journal of the American Statistical Association* 102.479, pp. 984–996. DOI: 10.1198/016214507000000527.

Thomas C.M. Lee (2003). “Smoothing parameter selection for smoothing splines: a simulation study”.
In: *Computational Statistics & Data Analysis* 42.1-2, pp. 139–148. DOI: [https://doi.org/10.1016/S0167-9473\(02\)00159-7](https://doi.org/10.1016/S0167-9473(02)00159-7).

Affidavit

"I hereby confirm that the work presented has been performed and interpreted solely by myself except for where I explicitly identified the contrary. I assure that this work has not been presented in any other form for the fulfillment of any other degree or qualification. Ideas taken from other works in letter and in spirit are identified in every single case."

Bonn, 11.02.2021 _____
Jonghun Baek

Bonn, 11.02.2021 _____
Jakob R. Juergens

Bonn, 11.02.2021 _____
Jonathan Willnow